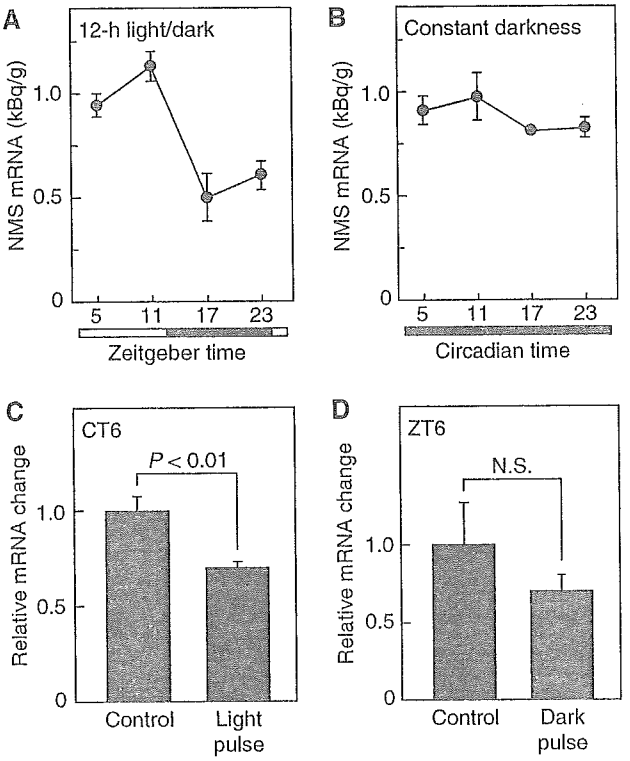

Figure 5 Expression pattern of rat NMS within the SCN. **(A, B)** Temporal expression profiles of the NMS mRNA. Animals were maintained under 12-h light/dark cycles (A) or constant darkness for 2 days (B). The amount of NMS mRNA was quantified by *in situ* hybridization analysis. The experiments were performed side by side. Data represent the means ± s.e.m. of 3–4 animals. Open and filled horizontal bars indicate light and dark periods, respectively. **(C, D)** Responses of NMS expression to light exposure under conditions of constant darkness and to a dark pulse during the light period of a 12-h light/dark cycle. Animals maintained in constant darkness for 2 days were exposed to a light pulse for 30 min at CT6 (C), or animals maintained under 12-h light/dark cycles were exposed to a dark pulse for 30 min at ZT6 (D). Brain samples were collected 1 h after exposure to the light or dark pulse. Data are presented as the means ± s.e.m. of 3–4 animals, and are shown as relative changes in NMS mRNA levels.

spinal cord by our group (Minamino *et al*, 1985). NMS shares a C-terminal core structure with NMU. The nucleotide sequences of the NMS and NMU cDNAs show low homology (53%) to each other. Genome database searches showed that, similar to the *NMU* gene (GenBank accession numbers AF222755–AF222765), the *NMS* gene is composed of 10 exons and the exon–intron boundaries in the NMS proprotein are comparably conserved with those in the NMU proprotein. Moreover, the domain structures of both proproteins are also similar, because the proteolytic processing sites are conserved. The structural similarities of NMS and NMU on the gene and proprotein levels were observed among mouse, rat and human, indicating that the divergence of the two genes encoding these peptides preceded the rodent/primate split during the process of evolution. In addition, the NMS proprotein contains another novel 34-residue peptide, similar to the novel 33-residue peptide that Lo *et al* (1992) speculated to exist in the NMU proprotein. Indeed, we purified such an endogenous 33-residue peptide derived from the NMU proprotein from rat brain and small intestine extracts. Both synthetic 33- and 34-residue peptides derived from the NMU and NMS proproteins show potent prolactin-releasing activity upon ICV administration in rats (Mori *et al*, in preparation).

Pharmacological characterization using CHO cells expressing receptors indicated that NMS and NMU share quite similar potency and efficacy for both recombinant FM-3/GPR66 and FM-4/TGR-1; these results were confirmed with another expression system using HEK293 cells (data not shown). However, it is interesting that ICV-administered NMS induced more potent phase shifting of circadian rhythm and suppression of feeding than ICV-administered NMU (Nakahara *et al*, 2004; Ida *et al*, in preparation), whereas both peptides showed similar effects on the contractile activities of chick rectum, and on elevation of systemic blood pressure. These results indicate that NMS showed more potent activity than NMU in the CNS but not in peripheral tissues. The pharmacological effects of NMS and NMU were different in the CNS, whereas the two peptides showed the same activity in peripheral tissues and in *in vitro* experiments. The molecular mechanisms of this difference remain unclear. The functional activity of receptors in the CNS may be modulated by unknown modifying molecules, such as receptor-activity-modifying proteins (McLatchie *et al*, 1998).

Because NMU is an anorexigenic neuropeptide involved in the central regulation of feeding behavior (Howard *et al*, 2000; Kojima *et al*, 2000; Hanada *et al*, 2004), NMS may also play a role in feeding regulation. However, unlike NMU, the NMS mRNA is expressed at only a low level in the PVN and arcuate nuclei, which are closely implicated in the regulation of this process (Schwartz *et al*, 2000). Further investigation of the physiological significance of NMS in the regulation of feeding behavior is needed, because the *NMS* gene was mapped to chromosome 2q11.2 in human, and this locus is consistent with one potential location of quantitative trait loci implicated in obesity (Barsh *et al*, 2000).

It has been well established that the circadian rhythm is generated by an endogenous pacemaker located in the SCN, and that precise, rhythmic oscillation of this pacemaker is coordinated by various neurochemical substances (Lowrey and Takahashi, 2000; Reppert and Weaver, 2001, 2002). The data obtained in this study strongly suggest that NMS functions as a regulator of the circadian pacemaker in an autocrine and/or paracrine manner within the SCN. The circadian rhythm can be phase shifted by photic and nonphotic stimuli, both of which contribute to important mechanisms in the entrainment of the circadian pacemaker (Mrosovsky, 1996; Lowrey and Takahashi, 2000). The SCN core receives photic and nonphotic environmental signals from the retina, the intergeniculate leaflet (IGL) of the lateral geniculate nuclei (LGN) and the median raphe of the brainstem, and consequently plays a crucial role in circadian entrainment (Reppert and Weaver, 2001). Several neuropeptides are implicated in the mechanism of circadian entrainment. For example, pituitary adenylate cyclase-activating polypeptide conveys photic signal via the retinohypothalamic tract (Hannibal, 2002). Neuropeptide Y in the geniculohypothalamic tract plays a role in mediating nonphotic signal from the IGL (Harrington, 1997). Neuropeptides intrinsic to the SCN also regulate the phase of the circadian rhythm. The VIP–$VPAC_2$ receptor system is important for photic entrainment and maintenance of the circadian rhythm (Piggins and Cutler, 2003). $VPAC_2$ receptor-deficient mice are incapable of sustaining normal

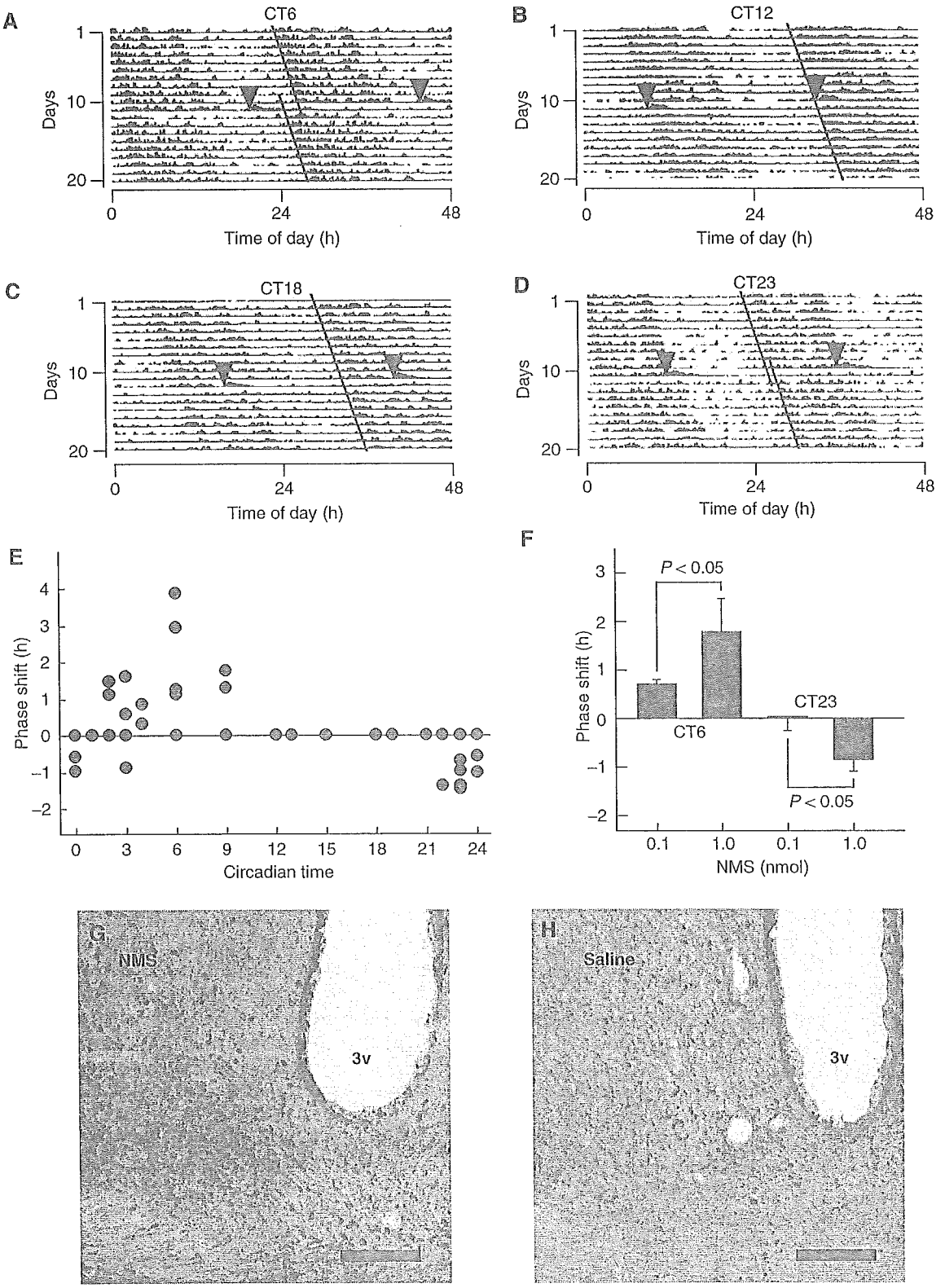

Figure 6 *In vivo* experiments with rat NMS. (**A–D**) Phase shifts of the circadian rhythm of locomotor activity induced by ICV administration of NMS. Representative doubled-plotted actograms of locomotor activity are shown. Rats were ICV administered with rat NMS (1 nmol) at CT6 (A), CT12 (B), CT18 (C) and CT23 (D). Each arrowhead indicates the time of NMS administration. Each line shows the regression lines drawn based on the daily onset of locomotor activity before and after administration. (**E**) Phase-response plot for ICV administration of 1 nmol NMS. The plus and minus values indicate phase advance and delay, respectively. $n = 3$–5. The data points at CT12, 13, 15, 18 and 19 overlap. (**F**) Dependence of circadian rhythm phase shift on NMS administration. ICV administration of NMS at CT6 and CT23 induced significant phase advance and delay, respectively, in a dose-dependent manner. $n = 4$–5 per group. (**G, H**) Induction of c-Fos protein expression within the SCN following ICV administration of NMS. Rats were administered at CT6 with 1 nmol NMS (G) or saline (H). 3v, third ventricle. Scale bar, 150 μm.

circadian rhythm of rest/activity behavior (Harmar *et al*, 2002). Loss of VIP/peptide histidine isoleucine in mice is sufficient to produce severe disruptions in the generation of circadian oscillations and the synchronization of these rhythms to the environment (Colwell *et al*, 2003). VIP is expressed in the SCN core and is released into the SCN shell to entrain the pacemaker. Similar to light pulses, application of VIP into the SCN results in a phase shift of the circadian rhythm during subjective night *in vivo* and *in vitro* (Piggins and Cutler, 2003). On the other hand, a neurotransmitter γ-aminobutylic acid, located in the SCN, LGN and IGL, is involved in nonphotic entrainment of the circadian rhythm (Turek and Van Reeth, 1988; Harrington, 1997). However, no SCN-intrinsic neuropeptides involved in this process have yet been identified. The expression of NMS in the SCN core suggests its involvement in circadian entrainment. In contrast to VIP, NMS induced phase shifts of the circadian rhythm of locomotor activity when tested during subjective day, and the PRC for NMS is very similar to that for nonphotic stimuli (Mrosovsky, 1996). These data suggest that NMS is a candidate for a nonphotic entrainment factor intrinsic to the SCN. Moreover, NMS, as well as VIP, may be involved in maintenance of the circadian rhythm.

The expression of NMS mRNA fluctuated within the SCN under light/dark cycling, but not under conditions of constant darkness. The expression was high during daytime and low at night, indicating that NMS expression is influenced by the light conditions. However, the NMS mRNA oscillation under light/dark cycling is not simply due to an enhancement of NMS gene expression by light, because the peak level of NMS mRNA during the light period is approximately the same as the levels throughout the day under conditions of constant darkness. Moreover, the NMS mRNA levels under constant darkness are not increased by light exposure at CT6, whereas the expression level is high during ZT5–11. Therefore, NMS expression is likely suppressed during the dark period of the light/dark cycle; this is consistent with the fact that a dark pulse at ZT6 tended to suppress the expression of NMS mRNA. It is well known that a cAMP responsive element (CRE) in the promoter regions of light responsive genes plays a crucial role in induction of gene expression by light in the SCN (Reppert and Weaver, 2001). The phosphorylation of CRE binding protein (CREB) at Ser 133 is required to activate the transcription of genes containing CRE (Gonzalez and Montminy, 1989). The light exposure induces CREB phosphorylation in the SCN during subjective night (CT19), but not during subjective day (CT6), suggesting that the components of the circadian pacemaker that gate light-sensitive molecular responsiveness in the SCN may act upstream of phosphorylation of CREB (Ginty *et al*, 1993). Computational analysis did not identify a CRE within the putative promoter region of the *NMS* gene (see Supplementary data). Therefore, it is natural that photic induction of the NMS expression at CT6 is not observed in the SCN. These data suggest that the expression of the NMS mRNA within the SCN is regulated indirectly by light under light/dark cycling. In addition, no CACGTG E-box element is found in the promoter region of the *NMS* gene (see Supplementary data). This element is closely involved in intrinsic circadian rhythmicity of gene expression (Reppert and Weaver, 2001). Therefore, the absence of a CACGTG E-box is consistent with the observation that no NMS mRNA oscillation is found under conditions of constant darkness, and supports the suggestion that the expression of NMS is not under the control of clock-gene families. As described above, NMS expression within the SCN shows a unique profile in response to light conditions. In particular, the NMS mRNA levels are suppressed by a light pulse at CT6. At present, it is not clear how the expression of the NMS mRNA is transcriptionally regulated in the SCN. The elucidation of this mechanism may provide novel insights into the regulatory mechanism of circadian oscillator systems.

Recently, our group reported that NMU is involved in the circadian oscillator system (Nakahara *et al*, 2004). Because NMS induces a circadian phase shift through same receptor with NMU within the SCN, it is no wonder that ICV administration of NMU also induces phase shifts. However, NMU is expressed in many discrete nuclei of the hypothalamus and the caudal brainstem (Howard *et al*, 2000), whereas NMS expression is restricted to the SCN. Furthermore, the magnitude of the phase shift induced by NMU is smaller than that caused by NMS. These facts suggest that NMS is a more specific and effective regulator of the circadian oscillator system than NMU.

The shapes of the NMS and NMU PRCs were subtly different. The magnitude of phase advance induced by NMS was larger than the magnitude of phase delay. In contrast, when NMU was ICV injected, phase delay was stronger than phase advance (Nakahara *et al*, 2004). Moreover, the maximum phase delays were caused by NMS and NMU when injected at CT23 and CT0, respectively, while the maximum phase advances were elicited by these peptides when injected at the same time (CT6). Two types of receptors for NMS and NMU are expressed in the SCN. The FM-4/TGR-1 mRNA has a nocturnal peak in its expression rhythm, whereas the expression of the FM-3/GPR66 mRNA peaks during daytime (Nakahara *et al*, 2004). Moreover, the receptor activities to the respective peptides may be modulated in the CNS as described above. Therefore, the difference in the PRC shapes for NMS and NMU may be due to the timing of receptor expression and different affinities of the receptors to the respective peptides in the CNS. On the other hand, the expression levels of NMS and NMU in the SCN are high during daytime and low at night. These rhythms are similar to the rhythm of FM-3/GPR66, and opposite to the rhythm of FM-4/TGR-1. Therefore, it is important to determine the endogenous peptide/receptor pairs and their efficiencies to elucidate the functional roles of NMS and NMU in the circadian oscillator system of the SCN. However, this is extremely difficult, because there are currently very few tools, such as specific antagonists, for analysis. This problem will be solved by engineering mice deficient for NMS, NMU or their receptors.

Light- and photic-related stimuli strongly elicit the expression of c-Fos protein in the SCN with a photic type phase shift (Castel *et al*, 1997). In contrast, c-Fos protein expression is not associated with phase shifts induced by nonphotic stimuli and related-substances, such as triazolam (Zhang *et al*, 1993). However, in our previous study (Nakahara *et al*, 2004) and in this study, ICV-administered NMS and NMU induced c-Fos expression in the SCN core, even though these peptides cause a nonphotic type phase shift. These data suggest that NMS and/or NMU may also be involved in SCN functions other than nonphotic entrainment of the

circadian rhythm. On the other hand, there is a report that nonphotic manipulations induce the expression of c-Fos protein in rat SCN (Edelstein and Amir, 1995). Therefore, further analysis is necessary to elucidate the significance of c-Fos expression in the SCN induced by ICV-administered NMS and NMU in the SCN.

Our group has previously demonstrated the specific expression of NMU in the SCN core (Nakahara *et al*, 2004). In contrast, Graham *et al* (2003) reported that the NMU mRNA is expressed in the shell of the SCN by *in situ* hybridization histochemistry. This disagrees with our results. We analyzed the distribution of NMU by immunohistochemistry using an antibody against rat NMU. Because this antibody was raised against the C-terminal amidated seven-residue structure of rat NMU, which is completely conserved in rat NMS (Honzawa *et al*, 1990), it is able to equally recognize both NMU and NMS, suggesting that the immunoreactivity we observed in the SCN core probably reflects the distribution of NMS. Therefore, we accept the specific expression of NMU in the SCN shell, although further analysis of the distribution of these peptides within the SCN is needed.

NMS and NMU probably play distinct roles in the circadian oscillator system. NMS may be involved in the regulation of circadian rhythm as described above, because the expression of the NMS mRNA in the core region of the SCN is not regulated by clock-gene families, indicating that NMS functions upstream of the endogenous circadian pacemaker. On the other hand, the expression of the NMU mRNA shows a circadian rhythm in the SCN shell of rats maintained under constant darkness (Graham *et al*, 2003; Nakahara *et al*, 2004), indicating that NMU, unlike NMS, is controlled by the endogenous pacemaker. Therefore, NMU may act either as a part of a central clock mechanism or as an output signal from the SCN, such as transforming growth factor-α (Kramer *et al*, 2001) and prokineticin 2 (Cheng *et al*, 2002). This speculation is supported by the phenotype of some NMU-deficient mice that have shown arrhythmicity in feeding behavior and locomotor activity (Hanada *et al*, 2004; Kojima *et al*, in preparation).

In conclusion, we have identified a novel 36-residue neuropeptide NMS, which was purified from rat brain extracts. The restricted expression of NMS in the SCN core and the ability of NMS to shift the phase of the circadian rhythm demonstrate that this newly identified peptide is important for the regulation of circadian rhythm. NMS is a candidate for a nonphotic entrainment factor of circadian rhythm. Our identification and characterization of NMS provide a foundation on which further research can build to provide novel insights into the regulatory mechanism of circadian rhythm.

Materials and methods

Establishment of cells expressing orphan GPCRs and assay system

Full-length cDNAs of human FM-3/GPR66 (GenBank accession number BC036543; residues 209–1420) and FM-4/TGR-1 (AF242874; residues 1–1240) were cloned into pcDNA3.1 vectors (Invitrogen) and transfected into CHO cells. The stably expressing cell lines (CHO/FM-3-14 and CHO/FM-4-16) that showed the highest change in $[Ca^{2+}]_i$ induced by human NMU were used in this study. The calcium-mobilization assay was carried out using the FLIPR system (Molecular Device) as described previously (Kojima *et al*, 1999). The test samples were dissolved in assay buffer containing 1% bovine serum albumin (BSA).

Purification of NMS

The peptide fraction (SP-III) was extracted from 420 rat brains (510 g) as described previously (Kojima *et al*, 1999), and then fractionated on a Sephadex G-50 gel filtration column (2.9 × 145 cm; Amersham Biosciences). A portion of each fraction equivalent to 1 g of tissue was subjected to assay using CHO/FM-4 cells. The active fraction was separated by carboxymethyl ion exchange HPLC on a TSK-gel CM-2SW column (4.6 × 250 mm; Tosoh) at pH 6.4. The activity was further purified by fractionation on the same column at pH 4.8. Finally, a single active peak was purified by successive RP-HPLCs on a Symmetry 300 C18 column (3.9 × 150 mm; Waters), a diphenyl column (2.1 × 150 mm, 219TP5215; Vydac) and a Chemcosorb 3ODS-H column (2.1 × 75 mm; Chemco). The primary structure was determined using a protein sequencer (494cLC; Applied Biosystems). The correct mass of the purified peptide was verified by matrix-assisted laser desorption/ionization time-of-flight mass spectrometry using a Voyager-DE PRO (Applied Biosystems).

Cloning of mouse, rat and human prepro-NMS cDNA

A tblastn search of the GenBank database was performed using the partial primary sequence of the purified peptide, and one mouse EST sequence (GenBank accession number BQ175462) was obtained. Based on this sequence, a full-length cDNA encoding mouse prepro-NMS was cloned from mouse hypothalamic poly(A)$^+$ RNA by RNA ligase-mediated rapid amplification of cDNA ends (RACE) using a GeneRacer kit (Invitrogen). The entire coding region of the cDNA was also amplified by nested PCR. The GenBank database was searched again using the mouse cDNA sequence, and the genomic sequences for the human and rat (AC068538 and AC096486, respectively) homologs were obtained. The entire coding regions of the human and rat cDNAs were amplified by nested PCR using human and rat brain Marathon Ready cDNAs (Clontech). All PCR reactions were conducted using the high-fidelity *Pyrobest* DNA polymerase (TaKaRa). The cDNA sequences were determined from six independent clones and were all completely identical to one another. The primer sequences used for cDNA cloning are listed in Tables I and II.

Receptor binding assay

Binding analysis was performed as described previously with slight modification (Gottschall *et al*, 1990). Plasma membranes isolated from CHO/FM-3 and CHO/FM-4 cells were incubated with 50 pM [^{125}I-Tyr^0]-human NMS and increasing concentrations of competitive peptide at room temperature for 2 h in binding buffer

Table I Primer sequences used in the cloning of mouse NMS cDNA by RACE

Name	Sequence
5′-RACE first	5′-GGAAAAATGGCCTCCCCAGG-3′
5′-RACE nested	5′-CCCAGGCTGGTAGTAGGATC-3′
3′-RACE first	5′-GGGAAATGCTCATCACCTCTCTGAACAG-3′
3′-RACE nested	5′-TCTGTGGTCTGCAAAGAGAATCCAGAGC-3′

Table II Primer sequences used in the cloning of mouse, rat and human NMS cDNAs by nested PCR

Species	PCR	Orientation	Sequence
Mouse	First	(+)	5′-TGCTCATCACCTCTCTGAACAG-3′
		(−)	5′-GCATGGGACAACAGAAATATGGC-3′
	Nested	(+)	5′-CTGTGGTCTGCAAAGAGAATCC-3′
		(−)	5′-CTCCAAAGGCGCACACCGTCTG-3′
Rat	First	(+)	5′-CTCTGCCTCTGGACCCTCG-3′
		(−)	5′-GCGTGGGACAGCAGAAATATGGT-3′
	Nested	(+)	5′-CTCATCTGTGGTCTGCAAAGAG-3′
		(−)	5′-CTCCAAAGATGCACACTGTCTT-3′
Human	First	(+)	5′-TGTCCTAGCAGCACCTGTCTGTG-3′
		(−)	5′-GAAGGCCTCATCAGATCCAG-3′
	Nested	(+)	5′-TGGCCAGCAAGGAGAAACCAGAC-3′
		(−)	5′-CAGATCCAGCTTTCTTTCACC-3′

(+), sense; (−), antisense.

containing 0.05% CHAPS and 1% BSA. Bound and free ligands were separated by filtration, and the radioactivity was measured using a TopCount liquid scintillation counter (Packard).

Quantitative RT–PCR

RNA was isolated from 8-week-old Wistar rats, and various brain regions were dissected as reported previously (Murakami and Takahashi, 1983). Quantitative RT–PCR was conducted with a LightCycler system (Roche) using a LightCycler-FastStart DNA Master SYBR Green I kit (Roche). The primer set used for rat NMS was 5′-CTCATCTGTGGTCTGCAAAGAG-3′ and 5′-GCATACA GAAGCAGTAGATGAC-3′. Known amounts of rat NMS cDNA were used to obtain a standard curve. Rat GAPDH mRNA was also measured as an internal control.

In situ hybridization histochemistry

In situ hybridization histochemistry was carried out on 12 μm coronal sections of whole rat brains as described previously (Ozaki *et al*, 2002). The following ^{35}S-labeled antisense oligonucleotides were used: 5′-TGAGGAGGGGATCTGTAGCATACAGAAGCA-3′ for NMS; 5′-GTGTCGTTTGACCGGCACGGGGTCTTCCG-3′ for VIP; and 5′-CAGCTCCCGGGCTGGCCCGTCCAGCT-3′ for AVP. Hybridized sections were apposed to autoradiography film. The autoradiographic images were quantified by an MCID imaging analyzer (Imaging Research) using a ^{14}C standard. Data were normalized with respect to the differences between signal intensities in equivalent areas of the SCN. The time-dependent profiles of expression were analyzed using one-way ANOVA followed by Scheffe's multiple comparisons test. The effects of light and dark pulses on expression levels were evaluated using one-way ANOVA with the *post hoc* Fisher's test.

Recording of rhythm of locomotor activity

Male Wistar rats (300–350 g) were used in this study. ICV administration was performed as described previously (Ida *et al*, 1999). Locomotor activity was measured as described previously (Nakahara *et al*, 2004). The phase shift in the rhythm of locomotor activity was calculated based on the distance between the two regression lines representing the daily onset of locomotor activity for at least 10 days before and after ICV administration of NMS or saline. The onset of locomotor activity was set as CT12. Phase-response data were evaluated using one-way ANOVA followed by Scheffe's multiple comparisons test. Dose-dependent effects were evaluated using one-way ANOVA with the *post hoc* Fisher's test.

Immunostaining for c-Fos protein

Rats were maintained under constant darkness for 2 weeks, and ICV administration of 1 nmol NMS or saline was performed at CT6. At 90 min after administration, rats were perfused with 2% paraformaldehyde. Immunostaining for c-Fos protein was performed as described previously (Date *et al*, 1999).

Supplementary data

Supplementary data are available at *The EMBO Journal* Online.

Acknowledgements

We thank JT Pearson for editing the manuscript, and H Kuwahara, Y Egi, H Okumura and M Miyazaki for technical assistance. This work was supported in part by the Program for Promotion of Fundamental Studies in Health Sciences of Pharmaceuticals and Medical Devices Agency (to KK), grant-in-aids from the Ministry of Education, Culture, Sports, Science and Technology of Japan (to KK, MM and MK), and the Program for the Promotion of Basic Research Activities for Innovative Bioscience (to NM and MK).

References

Barsh GS, Farooqi IS, O'Rahilly S (2000) Genetics of body-weight regulation. *Nature* **404**: 644–651

Brown DR, Quito FL (1988) Neuromedin U octapeptide alters ion transport in porcine jejunum. *Eur J Pharmacol* **155**: 159–162

Castel M, Belenky M, Cohen S, Wagner S, Schwartz WJ (1997) Light-induced c-Fos expression in the mouse suprachiasmatic nucleus: immunoelectron microscopy reveals co-localization in multiple cell types. *Eur J Neurosci* **9**: 1950–1960

Cheng MY, Bullock CM, Li C, Lee AG, Bermak JC, Belluzzi J, Weaver DR, Leslie FM, Zhou QY (2002) Prokineticin 2 transmits the behavioural circadian rhythm of the suprachiasmatic nucleus. *Nature* **417**: 405–410

Chu C, Jin Q, Kunitake T, Kato K, Nabekura T, Nakazato M, Kangawa K, Kannan H (2002) Cardiovascular actions of central neuromedin U in conscious rats. *Regul Peptides* **105**: 29–34

Civelli O, Nothacker HP, Saito Y, Wang Z, Lin SH, Reinscheid RK (2001) Novel neurotransmitters as natural ligands of orphan G-protein-coupled receptors. *Trends Neurosci* **24**: 230–237

Colwell CS, Michel S, Itri J, Rodriguez W, Tam J, Lelievre V, Hu Z, Liu X, Waschek JA (2003) Disrupted circadian rhythms in VIP- and PHI-deficient mice. *Am J Physiol Regul Integr Comp Physiol* **285**: R939–R949

Date Y, Ueta Y, Yamashita H, Yamaguchi H, Matsukura S, Kangawa K, Sakurai T, Yanagisawa M, Nakazato M (1999) Orexins, orexigenic hypothalamic peptides, interact with autonomic, neuroendocrine and neuroregulatory systems. *Proc Natl Acad Sci USA* **96**: 748–753

Edelstein K, Amir S (1995) Non-photic manipulations induce expression of Fos protein in the suprachiasmatic nucleus and intergeniculate leaflet in the rat. *Brain Res* **690**: 254–258

Fujii R, Hosoya M, Fukusumi S, Kawamata Y, Habata Y, Hinuma S, Onda H, Nishimura O, Fujino M (2000) Identification of neuromedin U as the cognate ligand of the orphan G protein-coupled receptor FM-3. *J Biol Chem* **275**: 21068–21074

Gardiner SM, Compton AM, Bennett T, Domin J, Bloom SR (1990) Regional hemodynamic effects of neuromedin U in conscious rats. *Am J Physiol* **258**: R32–R38

Ginty DD, Kornhauser JM, Thompson MA, Bading H, Mayo KE, Takahashi JS, Greenberg ME (1993) Regulation of CREB phosphorylation in the suprachiasmatic nucleus by light and a circadian clock. *Science* **260**: 238–241

Gonzalez GA, Montminy MR (1989) Cyclic AMP stimulates somatostatin gene transcription by phosphorylation of CREB at serine 133. *Cell* **59**: 675–680

Gottschall PE, Tatsuno I, Miyata A, Arimura A (1990) Characterization and distribution of binding sites for the hypothalamic peptide, pituitary adenylate cyclase-activating polypeptide. *Endocrinology* **127**: 272–277

Graham ES, Turnbull Y, Fotheringham P, Nilaweera K, Mercer JG, Morgan PJ, Barrett P (2003) Neuromedin U and neuromedin U receptor-2 expression in the mouse and rat hypothalamus: effects of nutritional status. *J Neurochem* **87**: 1165–1173

Hamada T, LeSauter J, Venuti JM, Silver R (2001) Expression of period genes: rhythmic and nonrhythmic compartments of the suprachiasmatic nucleus pacemaker. *J Neurosci* **21**: 7742–7750

Hanada R, Date Y, Shimbara T, Sakihara S, Murakami N, Hayashi Y, Kanai Y, Suda T, Kangawa K, Nakazato M (2003) Central action of neuromedin U via corticotropin-releasing hormone. *Biochem Biophys Res Commun* **311**: 954–958

Hanada R, Nakazato M, Murakami N, Sakihara S, Yoshimatsu H, Toshinai K, Hanada T, Suda T, Kangawa K, Matsukura S (2001) A role for neuromedin U in stress response. *Biochem Biophys Res Commun* **289**: 225–228

Hanada R, Teranishi H, Pearson JT, Kurokawa M, Hosoda H, Fukushima N, Fukue Y, Serino R, Fujihara H, Ueta Y, Ikawa M, Okabe M, Murakami N, Shirai M, Yoshimatsu H, Kangawa K, Kojima M (2004) Neuromedin U has a novel anorexigenic effect independent of the leptin signaling pathway. *Nat Med* **10**: 1067–1073

Hannibal J (2002) Neurotransmitters of the retino-hypothalamic tract. *Cell Tissue Res* **309**: 73–88

Harmar AJ, Marston HM, Shen S, Spratt C, West KM, Sheward WJ, Morrison CF, Dorin JR, Piggins HD, Reubi JC, Kelly JS, Maywood ES, Hastings MH (2002) The $VPAC_2$ receptor is essential for

circadian function in the mouse suprachiasmatic nuclei. *Cell* **109:** 497–508

Harrington ME (1997) The ventral lateral geniculate nucleus and the intergeniculate leaflet: interrelated structures in the visual and circadian systems. *Neurosci Biobehav Rev* **21:** 705–727

Hedrick JA, Morse K, Shan L, Qiao X, Pang L, Wang S, Laz T, Gustafson EL, Bayne M, Monsma Jr FJ (2000) Identification of a human gastrointestinal tract and immune system receptor for the peptide neuromedin U. *Mol Pharmacol* **58:** 870–875

Honzawa M, Sudoh T, Minamino N, Kangawa K, Matsuo H (1990) Neuromedin U-like immunoreactivity in rat intestine: regional distribution and immunohistochemical study. *Neuropeptides* **15:** 1–9

Hosoya M, Moriya T, Kawamata Y, Ohkubo S, Fujii R, Matsui H, Shintani Y, Fukusumi S, Habata Y, Hinuma S, Onda H, Nishimura O, Fujino M (2000) Identification and functional characterization of a novel subtype of neuromedin U receptor. *J Biol Chem* **275:** 29528–29532

Howard AD, Wang R, Pong SS, Mellin TN, Strack A, Guan XM, Zeng Z, Williams Jr DL, Feighner SD, Nunes CN, Murphy B, Stair JN, Yu H, Jiang Q, Clements MK, Tan CP, Mckee KK, Hreniuk DL, McDonald TP, Lynch KR, Evans JF, Austin CP, Caskey CT, Van der Ploeg LHT, Liu Q (2000) Identification of receptors for neuromedin U and its role in feeding. *Nature* **406:** 70–74

Ida T, Nakahara K, Katayama T, Murakami N, Nakazato M (1999) Effect of lateral cerebroventricular injection of the appetite-stimulating neuropeptide, orexin and neuropeptide Y, on the various behavioural activities of rats. *Brain Res* **821:** 526–529

Kojima M, Haruno R, Nakazato M, Date Y, Murakami N, Hanada R, Matsuo H, Kangawa K (2000) Purification and identification of neuromedin U as an endogenous ligand for an orphan receptor GPR66 (FM3). *Biochem Biophys Res Commun* **276:** 435–438

Kojima M, Hosoda H, Date Y, Nakazato M, Matsuo H, Kangawa K (1999) Ghrelin is a growth-hormone-releasing acylated peptide from stomach. *Nature* **402:** 656–660

Kramer A, Yang FC, Snodgrass P, Li X, Scammell TE, Davis FC, Weitz CJ (2001) Regulation of daily locomotor activity and sleep by hypothalamic EGF receptor signaling. *Science* **294:** 2511–2515

Lo G, Legon S, Austin C, Wallis S, Wang Z, Bloom SR (1992) Characterization of complementary DNA encoding the rat neuromedin U precursor. *Mol Endocrinol* **6:** 1538–1544

Lowrey PL, Takahashi JS (2000) Genetics of the mammalian circadian system: photic entrainment, circadian pacemaker mechanisms, and posttranslational regulation. *Annu Rev Genet* **34:** 533–562

McLatchie LM, Fraser NJ, Main MJ, Wise A, Brown J, Thompson N, Solari R, Lee MG, Foord SM (1998) RAMPs regulate the transport and ligand specificity of the calcitonin-receptor-like receptor. *Nature* **393:** 333–339

Minamino N, Kangawa K, Matsuo H (1985) Neuromedin U-8 and U-25: novel uterus stimulating and hypertensive peptides identified in porcine spinal cord. *Biochem Biophys Res Commun* **130:** 1078–1085

Moore RY, Speh JC, Leak RK (2002) Suprachiasmatic nucleus organization. *Cell Tissue Res* **309:** 89–98

Mrosovsky N (1996) Locomotor activity and non-photic influences on circadian clocks. *Biol Rev* **71:** 343–372

Murakami N, Takahashi K (1983) Circadian rhythm of adenosine-3′, 5′-monophosphate content in suprachiasmatic nucleus (SCN) and ventromedial hypothalamus (VMH) in the rat. *Brain Res* **276:** 297–304

Nakahara K, Hanada R, Murakami N, Teranishi H, Ohgusu H, Fukushima N, Moriyama M, Ida T, Kangawa K, Kojima M (2004) The gut-brain peptide neuromedin U is involved in the mammalian circadian oscillator system. *Biochem Biophys Res Commun* **318:** 156–161

Nakazato M, Hanada R, Murakami N, Date Y, Mondal MS, Kojima M, Yoshimatsu H, Kangawa K, Matsukura S (2000) Central effects of neuromedin U in the regulation of energy homeostasis. *Biochem Biophys Res Commun* **277:** 191–194

Ozaki Y, Onaka T, Nakazato M, Saito J, Kanemoto K, Matsumoto T, Ueta Y (2002) Centrally administered neuromedin U activates neurosecretion and induction of c-fos messenger ribonucleic acid in the paraventricular and supraoptic nuclei of rat. *Endocrinology* **143:** 4320–4329

Piggins HD, Cutler DJ (2003) The roles of vasoactive intestinal polypeptide in the mammalian circadian clock. *J Endocrinol* **177:** 7–15

Raddatz R, Wilson AE, Artymyshyn R, Bonini JA, Borowsky B, Boteju LW, Zhou S, Kouranova EV, Nagorny R, Guevarra MS, Dai M, Lerman GS, Vaysse PJ, Branchek TA, Gerald C, Forray C, Adham N (2000) Identification and characterization of two neuromedin U receptors differentially expressed in peripheral tissues and the central nervous system. *J Biol Chem* **275:** 32452–32459

Reppert SM, Weaver DR (2001) Molecular analysis of mammalian circadian rhythms. *Annu Rev Physiol* **63:** 647–676

Reppert SM, Weaver DR (2002) Coordination of circadian timing in mammals. *Nature* **418:** 935–941

Rouille Y, Duguay SJ, Lund K, Furuta M, Gong Q, Lipkind G, Oliva Jr AA, Chan SJ, Steiner DF (1995) Proteolytic processing mechanisms in the biosynthesis of neuroendocrine peptides: the subtilisin-like proprotein convertases. *Front Neuroendocrinol* **16:** 322–361

Schwartz MW, Woods SC, Porte Jr D, Seeley RJ, Baskin DG (2000) Central nervous system control of food intake. *Nature* **404:** 661–671

Sumi S, Inoue K, Kogire M, Doi R, Takaori K, Suzuki T, Yajima H, Tobe T (1987) Effect of synthetic neuromedin U-8 and U-25, novel peptides identified in porcine spinal cord, on splanchnic circulation in dogs. *Life Sci* **41:** 1585–1590

Turek FW, Van Reeth O (1988) Altering the mammalian circadian clock with the short-acting benzodiazepine, triazolam. *Trends Neurosci* **11:** 535–541

Vassilatis DK, Hohmann JG, Zeng H, Li F, Ranchalis JE, Mortrud MT, Brown A, Rodriguez SS, Weller JR, Wright AC, Bergmann JE, Gaitanaris GA (2003) The G protein-coupled receptor repertories of human and mouse. *Proc Natl Acad Sci USA* **100:** 4903–4908

von Heijne G (1986) A new method for predicting signal sequence cleavage site. *Nucleic Acids Res* **14:** 4683–4690

Wren AM, Small CJ, Abbott CR, Jethwa PH, Kennedy AR, Murphy KG, Stanley SA, Zollner AN, Ghatei MA, Bloom SR (2002) Hypothalamic actions of neuromedin U. *Endocrinology* **143:** 4227–4234

Zhang Y, Van Reeth O, Zee PC, Takahashi JS, Turek FW (1993) Fos protein expression in the circadian clock is not associated with phase shifts induced by a nonphotic stimulus, triazolam. *Neurosci Lett* **164:** 203–208

Transplantation of Mesenchymal Stem Cells Improves Cardiac Function in a Rat Model of Dilated Cardiomyopathy

Noritoshi Nagaya, MD; Kenji Kangawa, PhD; Takefumi Itoh, MD; Takashi Iwase, MD; Shinsuke Murakami, MD; Yoshinori Miyahara, MD; Takafumi Fujii, MD; Masaaki Uematsu, MD; Hajime Ohgushi, MD; Masakazu Yamagishi, MD; Takeshi Tokudome, MD; Hidezo Mori, MD; Kunio Miyatake, MD; Soichiro Kitamura, MD

Background—Pluripotent mesenchymal stem cells (MSCs) differentiate into a variety of cells, including cardiomyocytes and vascular endothelial cells. However, little information is available about the therapeutic potency of MSC transplantation in cases of dilated cardiomyopathy (DCM), an important cause of heart failure.

Methods and Results—We investigated whether transplanted MSCs induce myogenesis and angiogenesis and improve cardiac function in a rat model of DCM. MSCs were isolated from bone marrow aspirates of isogenic adult rats and expanded ex vivo. Cultured MSCs secreted large amounts of the angiogenic, antiapoptotic, and mitogenic factors vascular endothelial growth factor, hepatocyte growth factor, adrenomedullin, and insulin-like growth factor-1. Five weeks after immunization, MSCs or vehicle was injected into the myocardium. Some engrafted MSCs were positive for the cardiac markers desmin, cardiac troponin T, and connexin-43, whereas others formed vascular structures and were positive for von Willebrand factor or smooth muscle actin. Compared with vehicle injection, MSC transplantation significantly increased capillary density and decreased the collagen volume fraction in the myocardium, resulting in decreased left ventricular end-diastolic pressure (11 ± 1 versus 16 ± 1 mm Hg, $P<0.05$) and increased left ventricular maximum dP/dt (6767 ± 323 versus 5138 ± 280 mm Hg/s, $P<0.05$).

Conclusions—MSC transplantation improved cardiac function in a rat model of DCM, possibly through induction of myogenesis and angiogenesis, as well as by inhibition of myocardial fibrosis. The beneficial effects of MSCs might be mediated not only by their differentiation into cardiomyocytes and vascular cells but also by their ability to supply large amounts of angiogenic, antiapoptotic, and mitogenic factors. (*Circulation*. 2005;112:1128-1135.)

Key Words: myocytes ■ angiogenesis ■ heart failure ■ growth substances ■ transplantation

Despite advances in medical and surgical procedures, congestive heart failure remains a leading cause of cardiovascular morbidity and mortality.[1] Idiopathic dilated cardiomyopathy (DCM), a primary myocardial disease of unknown etiology characterized by a loss of cardiomyocytes and an increase in fibroblasts, is an important cause of heart failure.[2] Although myocyte mitosis and the presence of cardiac precursor cells in adult hearts have recently been reported,[3] the death of large numbers of cardiomyocytes results in the development of heart failure. Thus, restoring lost myocardium would be desirable for the treatment of DCM.

Mesenchymal stem cells (MSCs) are pluripotent, adult stem cells residing within the bone marrow microenvironment.[4] In contrast to their hematopoietic counterparts, MSCs are adherent and can be expanded in culture. MSCs can differentiate not only into osteoblasts, chondrocytes, neurons, and skeletal muscle cells but also into vascular endothelial cells[5] and cardiomyocytes.[6,7] In vitro, MSCs can be induced to differentiate into beating cardiomyocytes by 5-azacytidine treatment.[8] In vivo, MSCs directly injected into an infarcted heart have been shown to induce myocardial regeneration and improve cardiac function.[9] In addition, MSC implantation induces therapeutic angiogenesis in a rat model of hindlimb ischemia through vascular endothelial growth factor (VEGF) production by MSCs.[10,11] Myocardial blood flow abnormalities, even in the presence of angiographically normal coronary arteries, have been documented in patients with DCM.[12]

Received August 18, 2004; revision received April 28, 2005; accepted May 10, 2005.

From the Departments of Regenerative Medicine and Tissue Engineering (N.N., T.I., T.I., S.M.), Internal Medicine (N.N., M.Y., K.M.), Biochemistry (K.K., T.T.), and Cardiac Physiology (Y.M., T.F., H.M.), National Cardiovascular Center Research Institute, Osaka; the Cardiovascular Division (M.U.), Kansai Rosai Hospital, Hyogo; the Tissue Engineering Research Center (H.O.), National Institute of Advanced Industrial Science and Technology, Hyogo; and the Department of Cardiovascular Surgery (S.K.), National Cardiovascular Center, Osaka, Japan.

Reprint requests to Noritoshi Nagaya, MD, Department of Regenerative Medicine and Tissue Engineering, National Cardiovascular Center Research Institute, 5-7-1 Fujishirodai, Suita, Osaka 565-8565, Japan. E-mail nnagaya@ri.ncvc.go.jp

Circulation is available at http://www.circulationaha.org

DOI: 10.1161/CIRCULATIONAHA.104.500447

These findings raise the possibility that transplanted MSCs have beneficial effects on myocardial structure and function via myogenesis and angiogenesis. However, little information is available about the therapeutic potential of MSCs for DCM.

A unique model of myocarditis in the rat has been created by immunization with porcine cardiac myosin,[13] which results in severe heart failure characterized by increased cardiac fibrosis and left ventricular (LV) dilation.[14] Thus, the late phase of this model can serve as a model of DCM.

The purpose of this study was to investigate the following topics: (1) whether transplantation of MSCs induces myogenesis and angiogenesis, decreases collagen deposition in the myocardium, and thereby improves cardiac function in a rat model of DCM and (2) whether the beneficial effects of MSCs are mediated by their differentiation into cardiomyocytes and vascular cells and/or by their supplying angiogenic, antiapoptotic, and mitogenic factors.

Methods

Expansion of Bone Marrow MSCs

MSC expansion was performed according to previously described methods.[4] In brief, we humanely killed male Lewis rats and harvested bone marrow by flushing their femoral and tibial cavities with phosphate-buffered saline (PBS). Bone marrow cells were cultured in α-minimal essential medium supplemented with 10% fetal bovine serum and antibiotics. A small number of cells developed visible symmetric colonies by days 5 to 7. Nonadherent hematopoietic cells were removed, and the medium was replaced. The adherent, spindle-shaped MSC population expanded to $>5\times10^7$ cells within $\approx$4 to 5 passages after the cells were first plated.

Flow Cytometry

Cultured MSCs were analyzed by fluorescence-activated cell sorting (FACS) (FACScan flow cytometer, Becton Dickinson). Cells were incubated with fluorescein isothiocyanate (FITC)–conjugated mouse monoclonal antibodies against rat CD31 (clone TLD-3A12, Becton Dickinson), CD34 (clone ICO-115, Santa Cruz), CD45 (clone OX-1, Becton Dickinson), CD90 (clone OX-7, Becton Dickinson), vimentin (clone V9, Dako), and smooth muscle actin (SMA; clone 1A4, Dako). FITC-conjugated hamster anti-rat CD29 monoclonal antibody (clone Ha2/5, Becton Dickinson) and rabbit anti-rat c-Kit polyclonal antibody (clone C-19, Santa Cruz) were used. Isotype-identical antibodies served as controls.

Model of DCM

Male Lewis rats weighing 220 to 250 g (Japan SLC Inc, Hamamatsu, Japan) were used in this study. These isogenic rats served as donors and recipients of MSCs to simulate autologous implantation. DCM was produced by inducing experimental myocarditis, as described previously.[13,14] In brief, 1 mg (0.1 mL) of porcine heart myosin (Sigma) was mixed with an equal volume of Freund's complete adjuvant (Sigma) and injected into a footpad on days 1 and 7. Five weeks after immunization, these rats served as a model of heart failure due to DCM.

MSC Transplantation

In a preliminary experiment, we performed dose-response studies to obtain the maximal effects of cell transplantation. Because the effect of 10^6 MSCs was modest, we used 5×10^6 MSCs for transplantation. Five weeks after immunization, we injected a total of 5×10^6 MSCs/100 μL PBS, or PBS alone, into the myocardium at 10 points. In brief, the LV was divided into 3 levels (basal, middle, and apical). The basal and middle levels were each subdivided into 4 segments, and the apical level was subdivided into 2 segments. Injection into each segment was performed with a 27-gauge needle. Sham rats received intramyocardial injections of 100 μL PBS. This protocol resulted in the creation of 3 groups: DCM rats given MSCs (MSC-treated DCM group, n=10); DCM rats given PBS (untreated DCM group, n=10); and sham rats given PBS (sham group, n=10). The Animal Care Committee of the National Cardiovascular Center approved this experimental protocol.

Echocardiographic Studies

Echocardiographic studies were performed by an investigator, blinded to treatment allocation, at 5 weeks after immunization (before treatment) and 4 weeks after cell transplantation (after treatment). Two-dimensional, targeted M-mode tracings were obtained at the level of the papillary muscles with an echocardiographic system equipped with a 7.5-MHz transducer (HP Sonos 5500, Hewlett-Packard).[15] LV dimensions were measured according to the American Society for Echocardiology leading-edge method from at least 3 consecutive cardiac cycles. Fractional shortening was calculated as (LVDd−LVDs)/LVDd×100, where LVDd=LV diastolic dimension and LVDs=LV systolic dimension.

Hemodynamic Studies

Hemodynamic studies were performed 4 weeks after cell transplantation. A 1.5F micromanometer-tipped catheter (Millar Instruments) was inserted into the right carotid artery for measurement of mean arterial pressure.[16] Next, the catheter was advanced into the LV for measurement of LV pressure. Hemodynamic variables were measured with a pressure transducer (model P23 ID, Gould) connected to a polygraph. After completion of these measurements, the left and right ventricles were excised and weighed.

Histological Examination

To detect fibrosis in cardiac muscle, the LV myocardium (n=5 from each group) was fixed in 10% formalin, cut transversely, embedded in paraffin, and stained with Masson's trichrome. Transverse sections were randomly obtained from the 3 levels (basal, middle, and apical), and 20 randomly selected fields per section (n=60 per animal) were analyzed. After each field was scanned and computerized with a digital image analyzer (WinRoof, Mitani Co), collagen volume fraction was calculated as the sum of all areas containing connective tissue divided by the total area of the image.[15]

To detect capillaries in the myocardium, samples of harvested muscle (n=5 each) were embedded in OCT compound (Miles Scientific), snap-frozen in LN_2, cut into transverse sections, and stained for alkaline phosphatase by an indoxyltetrazolium method. Transverse sections were randomly obtained from the 3 levels (basal, middle, and apical), and 5 randomly selected fields per section (n=15 per animal) were analyzed. The number of capillaries was counted by light microscopy at a magnification of ×200. The number of capillaries in each field was averaged and expressed as the number of capillary vessels. These morphometric studies were performed by 2 examiners who were blinded to treatment assignment.

Assessment of Cell Differentiation

Suspended MSCs were labeled with fluorescent dyes with use of a PKH26 red fluorescent cell linker kit (Sigma), as reported previously.[17] Fluorescence-labeled MSCs were injected into the myocardium 5 weeks after immunization. Rats (n=5) were humanely killed 4 weeks after cell transplantation. LV samples were embedded in OCT compound, snap-frozen in LN_2, and cut into sections. Immunofluorescence staining was performed with monoclonal mouse anti-cardiac troponin T (Novo), anti-desmin (Dako), anti-connexin-43 (Sigma), polyclonal rabbit anti–von Willebrand factor (Dako), and monoclonal mouse SMA (Dako). FITC-conjugated IgG antibody (BD Pharmingen) was used as a secondary antibody. To perform quantitative analysis of the magnitude of MSC differentiation into cardiomyocytes, heart cells from each rat (n=5) were isolated by incubation in balanced salt solution containing 0.06% collagenase type II (Worthington Biochemical Co), as reported previously.[18] PKH26/troponin T double-positive cells were detected by FACS.

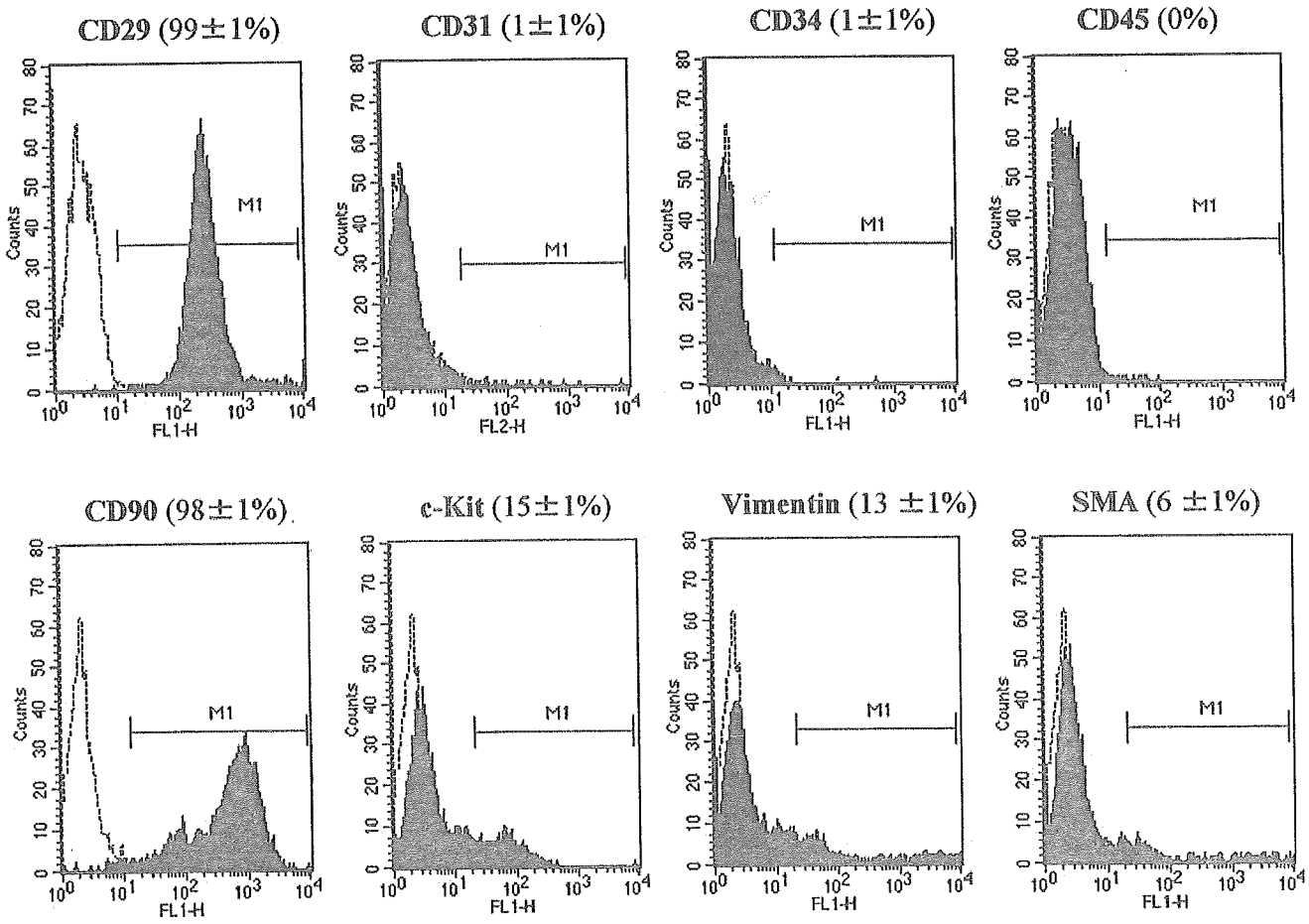

Figure 1. Flow-cytometric analysis of the adherent, spindle-shaped MSC population expanded to 4 to 5 passages. Most of the MSCs expressed CD29 and CD90, whereas they were negative for CD31, CD34, CD45, and SMA. Some of the cells were positive for c-Kit and vimentin.

Western Blot Analysis of Matrix Metalloproteinases

To identify the protein expression of matrix metalloproteinases (MMPs)-2 and -9, Western blotting was performed with rabbit polyclonal antibody raised against MMP-2 (Laboratory vision Co) and MMP-9 (Chemicon Co). The LV obtained from individual rats was used for comparison among the 3 groups (n=5 each). These samples were homogenized on ice in 0.1% Tween 20 homogenization buffer with a protease inhibitor. Then, 40 μg of protein was transferred into sample buffer, loaded on a 7.5% sodium dodecyl sulfate–polyacrylamide gel, and blotted onto a polyvinylidene fluoride membrane (Millipore Co). After being blocked for 120 minutes, the membrane was incubated with primary antibody at a dilution of 1:200. The membrane was incubated with peroxidase labeled with secondary antibody at a dilution of 1:1000. Positive protein bands were visualized with an ECL kit (Amersham) and measured by densitometry. Western blot analysis with a mouse polyclonal antibody raised against β-actin (Santa Cruz) was used as a protein loading control.

Assay for Angiogenic, Antiapoptotic, and Mitogenic Factors

To investigate whether MSCs produce angiogenic and growth factors, we measured VEGF, hepatocyte growth factor (HGF), insulin-like growth factor-1 (IGF-1), and adrenomedullin (AM) levels in conditioned medium 24 hours after medium replacement. VEGF, HGF, and IGF-1 were measured by enzyme immunoassay (VEGF immunoassay, R&D Systems Inc; rat HGF enzyme immunoassay, Institute of Immunology Co, Ltd; and active rat IGF-1 enzyme immunoassay, Diagnostic Systems Laboratories, Inc). AM level was measured with a radioimmunoassay kit (Shionogi Co), as reported previously.[19] The amounts of these products produced by MSCs were compared with those produced by bone marrow–derived mononuclear cells (MNCs) because MNCs have commonly been used for regenerative therapy.[19–21] There was no significant difference in cell viability between MSCs and MNCs 24 hours after seeding (88±5% versus 85±4% by trypan blue solution). In vivo, circulating levels of VEGF, HGF, IGF-1, and AM were measured before and 24 hours after administration of MSCs or vehicle (n=6 from each group).

Statistical Analysis

Numerical values are expressed as mean±SEM unless otherwise indicated. Comparisons of parameters between 2 groups were made with unpaired Student t test. Comparisons of parameters among 3 groups were made with a 1-way ANOVA, followed by the Scheffe multiple-comparison test. Comparisons of changes in parameters among the 3 groups were made by a 2-way ANOVA for repeated measures, followed by the Scheffe multiple-comparison test. A value of $P<0.05$ was considered significant.

Results

Characterization of Cultured MSCs

Most cultured MSCs expressed CD29 and CD90 (Figure 1). In contrast, the majority of MSCs were negative for CD31, CD34, CD45, and SMA. Some of the MSCs expressed c-Kit and vimentin.

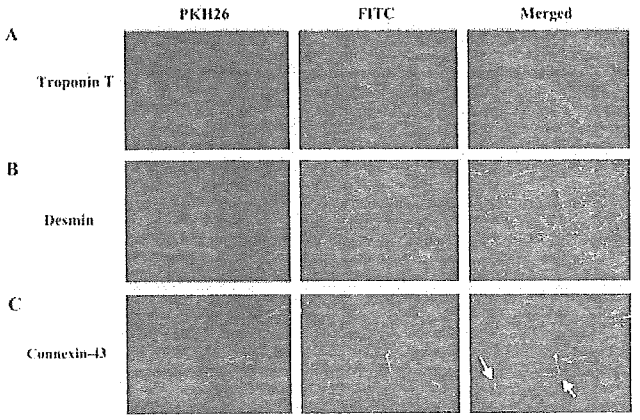

Figure 2. Differentiation of transplanted MSCs into cardiomyocytes. Transplanted MSCs were engrafted in the myocardium and stained for cardiac troponin T (A) and desmin (B). Engrafted MSCs also expressed connexin-43, a gap junction protein, at contact points with native cardiac myocytes (left arrow) and other transplanted cells (right arrow) (C). Magnification ×400.

Myogenesis and Angiogenesis Induced by MSCs

Red fluorescence–labeled MSCs were transplanted into the myocardium 5 weeks after immunization. Four weeks after transplantation, MSCs were engrafted into the myocardium (Figure 2). Immunofluorescence demonstrated that transplanted MSCs were positive for the cardiac markers cardiac troponin T and desmin (Figure 2). Transplanted MSCs also expressed connexin-43, a gap junction protein, at contact points with native cardiac myocytes as well as with MSCs. FACS analysis of isolated heart cells demonstrated that 8±1% of transplanted MSCs were double-positive for PKH26 and troponin T. These results suggest that a small number of transplanted MSCs can differentiate into cardiomyocytes.

Some transplanted MSCs formed vascular structures in the myocardium and were positive for von Willebrand factor (Figure 3A). Other MSCs were positive for SMA and participated in vessel formation as mural cells (Figure 3B). Alkaline phosphatase staining of the ischemic myocardium showed marked augmentation of neovascularization in the MSC-treated DCM group (Figures 4A–4C). Quantitative analysis demonstrated that capillary density was significantly

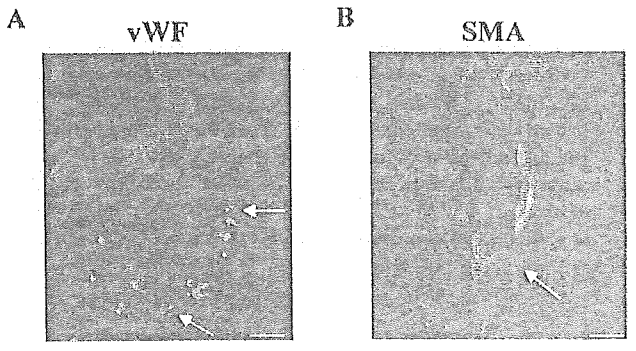

Figure 3. Differentiation of transplanted MSCs into vascular endothelial cells and smooth muscle cells. Some of the transplanted MSCs were positive for von Willebrand factor (vWF, A) and SMA (B) and formed vascular structures (A and B). Scale bars=10 μm.

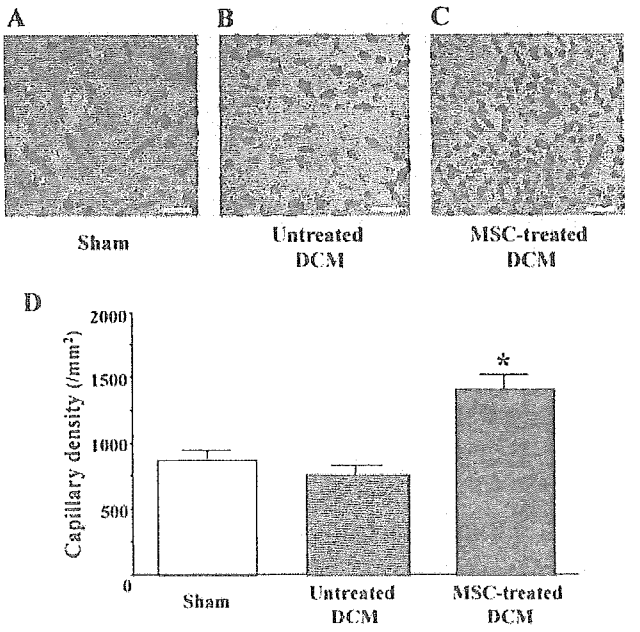

Figure 4. A–C, Representative samples of alkaline phosphatase staining of myocardium. Magnification, ×200. Scale bars=10 μm. D, Quantitative analysis of capillary density in the myocardium. Data are mean±SEM *P<0.05 vs untreated DCM group.

higher in the MSC-treated DCM group than in the untreated DCM group (Figure 4D).

Angiogenic, Antiapoptotic, and Mitogenic Factors Released From MSCs

After 24 hours of culture, MSCs secreted large amounts of angiogenic and antiapoptotic factors, including VEGF, HGF, and AM (Figure 5). Compared with MNCs that have commonly been used for regenerative therapy,[20–22] MSCs secreted 4-fold more VEGF and 5-fold more HGF. Similarly, MSCs secreted 6-fold more AM, an angiogenic and antiapoptotic peptide, compared with MNCs. MSCs also secreted a large amount, 10-fold greater than MNCs, of IGF-1, a growth hormone mediator for myocardial growth (Figure 5). Transplantation of MSCs significantly increased circulating VEGF (45.8±1.6 to 68.5±3.6 pg/mL, P<0.05), HGF (431.8±56.6 to 517.2±67.1 pg/mL, P<0.05), and AM (23.4±0.8 to 41.2±4.8 pg/mL, P<0.05) 24 hours after transplantation, although vehicle injection did not alter these parameters. Serum IGF-1 tended to increase after MSC transplantation (938.1±151.6 to 1063.5±116.9 pg/mL, P=NS), but this increase did not reach statistical significance.

Hemodynamic Effects of MSC Transplantation

Nine weeks after immunization, LV end-diastolic pressure showed a marked elevation in the untreated DCM group; this elevation was significantly attenuated in the MSC-treated DCM group (Figure 6A). LV maximum *dP/dt* was significantly lower in the untreated DCM group than in the sham group (Figure 6B). However, LV maximum *dP/dt* was significantly improved 4 weeks after MSC transplantation. There was no significant difference in heart rate or mean arterial pressure among the 3 groups (the Table). Echocardiographic studies demonstrated LV dysfunction and dilation

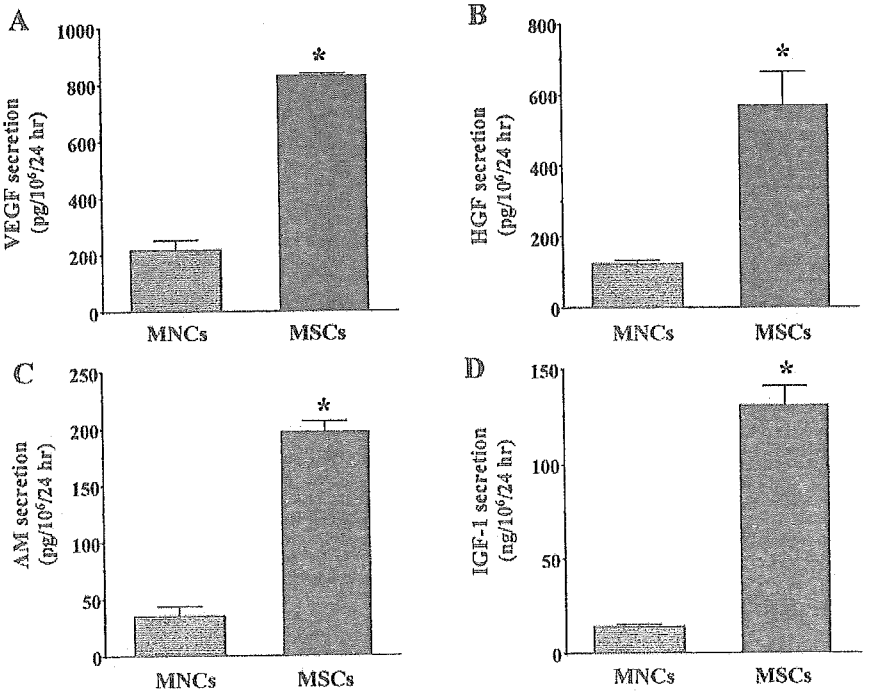

Figure 5. A–D, Angiogenic, antiapoptotic, and mitogenic factors produced by MSCs and bone marrow–derived MNCs). Compared with MNCs, MSCs secreted large amounts of VEGF, HGF, AM, and IGF-1. *$P<0.05$ vs MNCs.

in the untreated DCM group, as indicated by a decrease in percent fractional shortening and an increase in LV diastolic dimension (Figure 6C and 6D). However, MSC transplantation increased percent fractional shortening and inhibited the increase in LV diastolic dimension.

Reduction of Myocardial Fibrosis by MSC Transplantation

Masson's trichrome staining demonstrated modest myocardial fibrosis in the untreated DCM group (Figure 7A). However, MSC transplantation significantly attenuated the development of myocardial fibrosis. Quantitative analysis also demonstrated that the collagen volume fraction in the MSC-treated DCM group was significantly smaller than that in the untreated DCM group (Figure 7B). Western blot analysis showed that myocardial contents of MMP-2 and MMP-9 in the untreated DCM were significantly increased compared with those in the sham group (Figure 7C–E). However, the increases in MMP-2 and MMP-9 levels were attenuated by MSC transplantation, although the change in MMP-9 did not reach statistical significance.

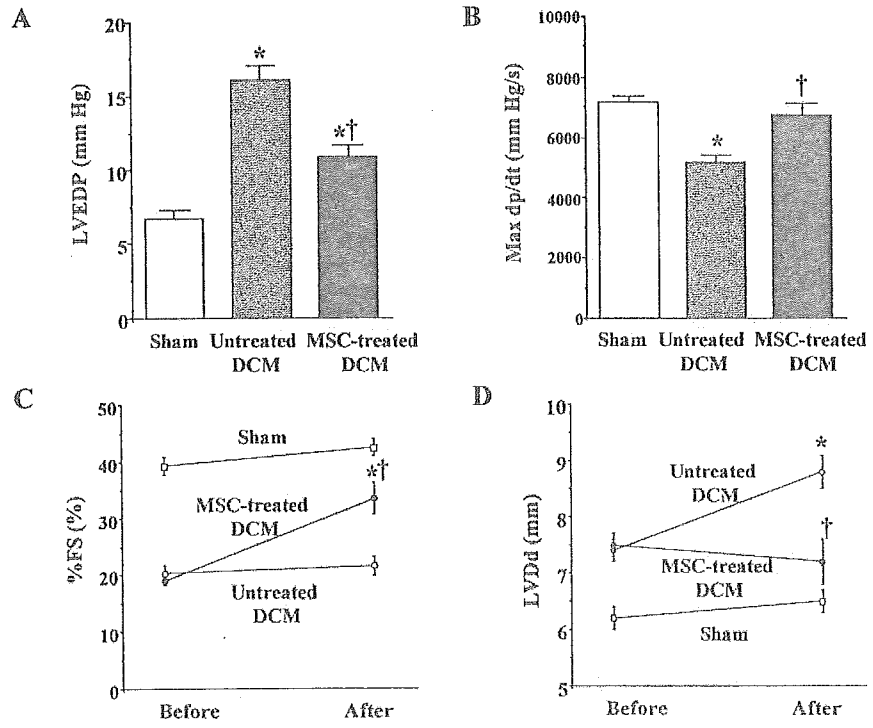

Figure 6. A and B, Effects of MSC transplantation on hemodynamic parameters. LVEDP indicates LV end-diastolic pressure; Max *dP/dt*, LV maximum *dP/dt*. Data are mean±SEM. *$P<0.05$ vs sham group; †$P<0.05$ vs untreated DCM group. C and D, Changes in echocardiographic parameters induced by MSC transplantation. %FS indicates LV fractional shortening. Data are mean±SEM *$P<0.05$ vs before transplantation; †$P<0.05$ vs the time-matched untreated DCM group.

Physiological Profiles of the 3 Experimental Groups

	Sham	Untreated DCM	MSC-Treated DCM
n	10	10	10
Body wt, g	421±8	372±4*	389±5*
LV wt/body wt, g/kg	1.91±0.05	2.18±0.06*	2.05±0.05
RV wt/body wt, g/kg	0.55±0.01	0.68±0.02*	0.60±0.03†
Heart rate, bpm	403±10	432±15	417±12
Mean arterial pressure, mm Hg	134±2	123±3	132±5

wt indicates weight; RV, right ventricle. Sham-operated rats were given vehicle only. The untreated DCM group included DCM rats treated with vehicle. The MSC-treated DCM group included DCM rats treated with MSCs. Data are mean±SEM.

*$P<0.05$ vs sham group; †$P<0.05$ vs untreated DCM group.

Discussion

In the present study, we have demonstrated the following effects of MSC transplantation in a rat model of DCM: (1) induction of myogenesis and angiogenesis; (2) differentiation of transplanted MSCs into cardiomyocytes, vascular endothelial cells, and smooth muscle cells; (3) secretion of large amounts of VEGF, HGF, AM, and IGF-1; (4) improvement of cardiac function and inhibition of ventricular remodeling; and (5) decrease in collagen volume fraction in the myocardium.

Earlier studies have shown that transplantation of MSCs improves cardiac function in experimental models of ischemic heart disease.[9,23] However, little information is available about the therapeutic potential of MSCs for chronic heart failure due to DCM. Previous studies have shown that porcine cardiac myosin-induced myocarditis progresses to a chronic phase resembling DCM.[13,14] Thus, we used this model 5 weeks after immunization as an example of experimental DCM.

In the present study, transplanted MSCs were engrafted into the myocardium in a rat model of DCM. Four weeks after transplantation, some of the engrafted MSCs were positively stained for cardiac troponin T and desmin. Transplanted MSCs also expressed connexin-43, a gap junction protein, at contact points with native cardiac myocytes as well as with MSCs. These results suggest that MSCs differentiate into cardiomyocytes in the myocardium and form connections with native cardiomyocytes in rats with DCM. Unlike earlier studies that have used a model of myocardial infarction,[7,9,23] we used a rat model of DCM to demonstrate the engraftment and cardiogenic differentiation of MSCs. Importantly, MSC transplantation improved cardiac function in these rats, as indicated by a significant decrease in LV end-diastolic pressure and an increase in LV dP/dt_{max}. Thus, the improvement in cardiac function may be a result of MSC-induced myocardial regeneration; however, further studies are necessary to investigate the mechanisms by which MSCs develop into cardiac myocyte–like cells.

Some of the transplanted MSCs were positive for a vascular endothelial cell marker and participated in vessel formation. MSC transplantation significantly increased capillary density in the myocardium. SMA staining revealed that MSCs differentiated into vascular smooth muscle cells, which play an important role in vessel maturation. Earlier studies have shown that transplantation of MNCs induces therapeutic angiogenesis in patients with limb ischemia or ischemic heart disease.[20–22] The angiogenic potential of MNCs is mediated at least in part by production by the cells of a variety of angiogenic factors.[24] Although MSCs have also been shown to produce VEGF,[10,25] there has been no study to compare their production between MSCs and MNCs. The present study demonstrated that MSCs secreted ≈4-fold more VEGF compared with MNCs. Furthermore, MSCs secreted large amounts of HGF and AM, potent angiogenic factors.[26–30] Taking these findings together, MSCs may contribute to neovascularization in the myocardium not only through their ability to generate capillary-like structures but also through growth factor–mediated paracrine regulation. Myocardial blood flow abnormalities have been documented in patients with heart failure caused by DCM.[12] Thus, it is possible that MSC-induced neovascularization contributes to improvement in cardiac function.

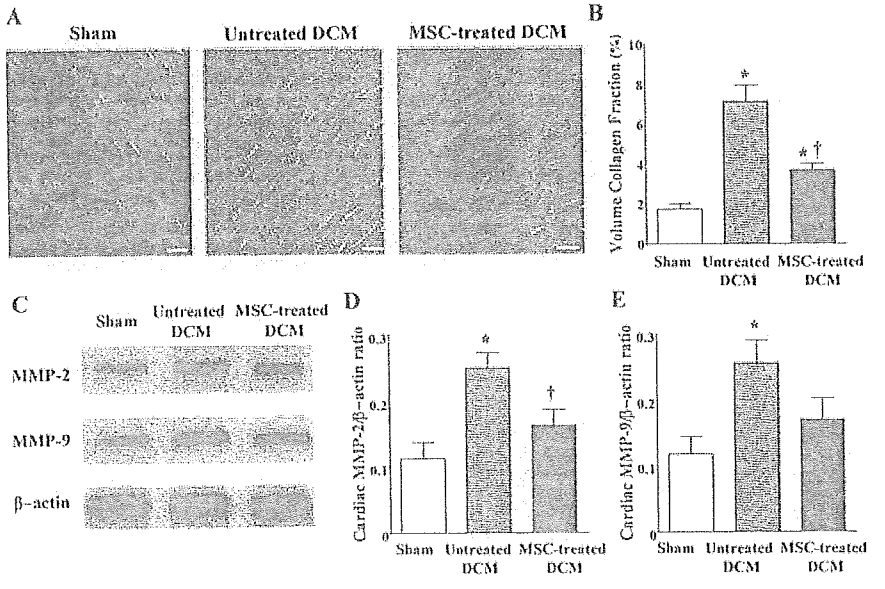

Figure 7. Effects of MSC transplantation on myocardial fibrosis. A, Photomicrographs show representative myocardial sections stained with Masson's trichrome. Scale bars=10 μm. B, Quantitative analysis demonstrated that the collagen volume fraction in the MSC-treated DCM group was significantly smaller than that in the untreated DCM group. C, Representative Western blots for MMPs-2 and -9 and β-actin in the heart. D and E, Quantitative analysis of cardiac tissue contents of MMP-2 and -9. Data are mean±SEM *$P<0.05$ vs sham group; †$P<0.05$ vs untreated DCM group.

HGF has not only angiogenic but also cardioprotective effects, including antiapoptotic, mitogenic, and antifibrotic activities.[26,27] *HGF* gene transfer into the myocardium improves myocardial function and geometry.[28] In particular, the antifibrotic effects of HGF through inhibition of transforming growth factor-β expression is beneficial for heart failure. Cultured MSCs secreted a large amount of HGF. In vivo, transplantation of MSCs slightly increased plasma HGF in rats. It significantly attenuated the development of myocardial fibrosis in a rat model of DCM. These results suggest that MSC-derived HGF may contribute to improvements in cardiac function partly through its antifibrotic effects.

MSCs also produced AM, a potent vasodilator and cardioprotective peptide.[29] We have shown that AM prevents cardiomyocyte apoptosis through the phosphatidylinositol 3-kinase/Akt–dependent pathway[16] and that it has potent angiogenic effects.[30] AM inhibits proliferation of cardiac fibroblasts through the cAMP-dependent pathway.[31] Administration of AM inhibits LV remodeling and improves cardiac function in heart failure.[32–34] In the present study, cultured MSCs secreted a large amount of AM in vitro. In vivo, transplantation of MSCs markedly increased plasma AM level. Taken together, these findings suggest that MSCs may exert their cardioprotective effects through AM-mediated paracrine regulation.

IGF-1, a growth hormone mediator, plays an important role in myocardial and skeletal muscle growth.[35,36] Administration of IGF-1 improves cardiac function after myocardial infarction through enhancement of myocardial growth.[37] Its protective and antiapoptotic properties have been demonstrated in different models of myocardial ischemia.[38] Furthermore, IGF-1 exerts Ca^{2+}-dependent, positive inotropic effects through a phosphatidylinositol 3-kinase–dependent pathway.[39] Interestingly, the present study demonstrated that MSCs secreted significant amounts of IGF-1 in vitro, 10-fold greater than MNCs. These findings raise the possibility that MSC-derived IGF-1 may participate in myocardial growth and enhancement of myocardial contractility in a rat model of DCM.

MMPs also play a crucial role in extracellular remodeling in heart failure.[40] In fact, pharmacological inhibition of MMP activities prevents progressive LV remodeling in an animal model of heart failure.[41] In the present study, cardiac MMP-2 and MMP-9 were increased in rats with DCM, which is consistent with recent findings in patients with heart failure.[40,42] Interestingly, MSC transplantation attenuated the increases in cardiac MMP-2 and MMP-9 in a rat model of DCM. Although the underlying mechanisms remain unclear, MSC transplantation may influence extracellular remodeling in heart failure.

The present study has some limitations. First, immunohistochemical evidence suggests differentiation of MSCs into cardiomyocytes, vascular endothelial cells, and smooth muscle cells. However, further studies are necessary to convincingly demonstrate differentiation of MSCs into a specific cell type. Second, the model of DCM used in this study was an injury model, and the effects of treatment may be related to attenuation of the injury rather than to the established cardiomyopathy. Nonetheless, the experiment was performed 5 to 9 weeks after myosin injection, by which time inflammatory changes were hardly observed and had been replaced by fibrosis.[43]

Conclusions

MSC transplantation improved cardiac function in a rat model of DCM, possibly through induction of myogenesis and angiogenesis, as well as by inhibition of myocardial fibrosis. The beneficial effects of MSCs may be mediated at least in part by their differentiation into cardiomyocytes and vascular cells and by their ability to supply large amounts of angiogenic, antiapoptotic, and mitogenic factors. Thus, MSC transplantation has potential as a new therapeutic strategy for the treatment of DCM.

Acknowledgments

This work was supported by research grants for cardiovascular disease (16C-6) and Human Genome Tissue Engineering 009 from the Ministry of Health, Labor and Welfare; the Industrial Technology Research Grant Program in '03 from the New Energy and Industrial Technology Development Organization of Japan; a research grant from the Japan Cardiovascular Research Foundation; and Promotion of Fundamental Studies in Health Science of the Organization for Pharmaceutical Safety and Research of Japan.

References

1. Cohn JN. The management of chronic heart failure. *N Engl J Med.* 1996;335:490–498.
2. Dec GW, Fuster V. Idiopathic dilated cardiomyopathy. *N Engl J Med.* 1994;331:1564–1575.
3. Beltrami AP, Urbanek K, Kajstura J, Yan SM, Finato N, Bussani R, Nadal-Ginard B, Silvestri F, Leri A, Beltrami CA, Anversa P. Evidence that human cardiac myocytes divide after myocardial infarction. *N Engl J Med.* 2001;344:1750–1757.
4. Pittenger MF, Mackay AM, Beck SC, Jaiswal RK, Douglas R, Mosca JD, Moorman MA, Simonetti DW, Craig S, Marshak DR. Multilineage potential of adult human mesenchymal stem cells. *Science.* 1999;284:143–147.
5. Reyes M, Dudek A, Jahagirdar B, Koodie L, Marker PH, Verfaillie CM. Origin of endothelial progenitors in human postnatal bone marrow. *J Clin Invest.* 2002;109:337–346.
6. Toma C, Pittenger MF, Cahill KS, Byrne BJ, Kessler PD. Human mesenchymal stem cells differentiate to a cardiomyocyte phenotype in the adult murine heart. *Circulation.* 2002;105:93–98.
7. Mangi AA, Noiseux N, Kong D, He H, Rezvani M, Ingwall JS, Dzau VJ. Mesenchymal stem cells modified with Akt prevent remodeling and restore performance of infarcted hearts. *Nat Med.* 2003;9:1195–1201.
8. Makino S, Fukuda K, Miyoshi S, Konishi F, Kodama H, Pan J, Sano M, Takahashi T, Hori S, Abe H, Hata J, Umezawa A, Ogawa S. Cardiomyocytes can be generated from marrow stromal cells in vitro. *J Clin Invest.* 1999;103:697–705.
9. Shake JG, Gruber PJ, Baumgartner WA, Senechal G, Meyers J, Redmond JM, Pittenger MF, Martin BJ. Mesenchymal stem cell implantation in a swine myocardial infarct model: engraftment and functional effects. *Ann Thorac Surg.* 2002;73:1919–1925.
10. Al-Khaldi A, Al-Sabti H, Galipeau J, Lachapelle K. Therapeutic angiogenesis using autologous bone marrow stromal cells: improved blood flow in a chronic limb ischemia model. *Ann Thorac Surg.* 2003;75:204–209.
11. Al-Khaldi A, Eliopoulos N, Martineau D, Lejeune L, Lachapelle K, Galipeau J. Postnatal bone marrow stromal cells elicit a potent VEGF-dependent neoangiogenic response in vivo. *Gene Ther.* 2003;10:621–629.
12. Parodi O, De Maria R, Oltrona L, Testa R, Sambuceti G, Roghi A, Merli M, Belingheri L, Accinni R, Spinelli F, Pellegrini A, Baroldi G. Myocardial blood flow distribution in patients with ischemic heart disease or dilated cardiomyopathy undergoing heart transplantation. *Circulation.* 1993;88:509–522.
13. Kodama M, Zhang S, Hanawa H, Saeki M, Inomata T, Suzuki K, Koyama S, Shibata A. Effects of 15-deoxyspergualin on experimental autoimmune giant cell myocarditis of the rat. *Circulation.* 1995;91:1116–1122.
14. Watanabe K, Ohta Y, Nakazawa M, Higuchi H, Hasegawa G, Naito M, Fuse K, Ito M, Hirono S, Tanabe N, Hanawa H, Kato K, Kodama M, Aizawa Y. Low dose carvedilol inhibits progression of heart failure in rats with dilated cardiomyopathy. *Br J Pharmacol.* 2000;130:1489–1495.

15. Nagaya N, Uematsu M, Kojima M, Ikeda Y, Yoshihara F, Shimizu W, Hosoda H, Hirota Y, Ishida H, Mori H, Kangawa K. Chronic administration of ghrelin improves left ventricular dysfunction and attenuates development of cardiac cachexia in rats with heart failure. *Circulation.* 2001;104:1430–1435.
16. Okumura H, Nagaya N, Itoh T, Okano I, Hino J, Mori K, Tsukamoto Y, Ishibashi-Ueda H, Miwa S, Tambara K, Toyokuni S, Yutani C, Kangawa K. Adrenomedullin infusion attenuates myocardial ischemia/reperfusion injury through the phosphatidylinositol 3-kinase/Akt-dependent pathway. *Circulation.* 2004;109:242–248.
17. Messina LM, Podrazik RM, Whitehill TA, Ekhterae D, Brothers TE, Wilson JM, Burkel WE, Stanley JC. Adhesion and incorporation of lacZ-transduced endothelial cells into the intact capillary wall in the rat. *Proc Natl Acad Sci U S A.* 1992;89:12018–12022.
18. Harada M, Itoh H, Nakagawa O, Ogawa Y, Miyamoto Y, Kuwahara K, Ogawa E, Igaki T, Yamashita J, Masuda I, Yoshimasa T, Tanaka I, Saito Y, Nakao K. Significance of ventricular myocytes and nonmyocytes interaction during cardiocyte hypertrophy: evidence for endothelin-1 as a paracrine hypertrophic factor from cardiac nonmyocytes. *Circulation.* 1997;96:3737–3744.
19. Ohta H, Tsuji T, Asai S, Sasakura K, Teraoka H, Kitamura K, Kangawa K. A simple immunoradiometric assay for measuring the entire molecules of adrenomedullin in human plasma. *Clin Chim Acta.* 1999;287:B131–B143.
20. Murohara T, Ikeda H, Duan J, Shintani S, Sasaki K, Eguchi H, Onitsuka I, Matsui K, Imaizumi T. Transplanted cord blood-derived endothelial precursor cells augment postnatal neovascularization. *J Clin Invest.* 2000; 105:1527–1536.
21. Tateishi-Yuyama E, Matsubara H, Murohara T, Ikeda U, Shintani S, Masaki H, Amano K, Kishimoto Y, Yoshimoto K, Akashi H, Shimada K, Iwasaka T, Imaizumi T. Therapeutic Angiogenesis using Cell Transplantation (TACT) Study Investigators. Therapeutic angiogenesis for patients with limb ischaemia by autologous transplantation of bone-marrow cells: a pilot study and a randomised controlled trial. *Lancet.* 2002;360:427–435.
22. Tse HF, Kwong YL, Chan JK, Lo G, Ho CL, Lau CP. Angiogenesis in ischaemic myocardium by intramyocardial autologous bone marrow mononuclear cell implantation. *Lancet.* 2003;4:47–49.
23. Min JY, Sullivan MF, Yang Y, Zhang JP, Converso KL, Morgan JP, Xiao YF. Significant improvement of heart function by cotransplantation of human mesenchymal stem cells and fetal cardiomyocytes in postinfarcted pigs. *Ann Thorac Surg.* 2002;74:1568–1575.
24. Kamihata H, Matsubara H, Nishiue T, Fujiyama S, Tsutsumi Y, Ozono R, Masaki H, Mori Y, Iba O, Tateishi E, Kosaki A, Shintani S, Murohara T, Imaizumi T, Iwasaka T. Implantation of bone marrow mononuclear cells into ischemic myocardium enhances collateral perfusion and regional function via side supply of angioblasts, angiogenic ligands, and cytokines. *Circulation.* 2001;104:1046–1052.
25. Kinnaird T, Stabile E, Burnett MS, Lee CW, Barr S, Fuchs S, Epstein SE. Marrow-derived stromal cells express genes encoding a broad spectrum of arteriogenic cytokines and promote in vitro and in vivo arteriogenesis through paracrine mechanisms. *Circ Res.* 2004;94:678–685.
26. Nakamura T, Nishizawa T, Hagiya M, Seki T, Shimonishi M, Sugimura A, Tashiro K, Shimizu S. Molecular cloning and expression of human hepatocyte growth factor. *Nature.* 1989;342:440–443.
27. Nakamura T, Mizuno S, Matsumoto K, Sawa Y, Matsuda H, Nakamura T. Myocardial protection from ischemia/reperfusion injury by endogenous and exogenous HGF. *J Clin Invest.* 2000;106:1511–1519.
28. Li Y, Takemura G, Kosai K, Yuge K, Nagano S, Esaki M, Goto K, Takahashi T, Hayakawa K, Koda M, Kawase Y, Maruyama R, Okada H, Minatoguchi S, Mizuguchi H, Fujiwara T, Fujiwara H. Postinfarction treatment with an adenoviral vector expressing hepatocyte growth factor relieves chronic left ventricular remodeling and dysfunction in mice. *Circulation.* 2003;107:2499–2506.
29. Kitamura K, Kangawa K, Kawamoto M, Ichiki Y, Nakamura S, Matsuo H, Eto T. Adrenomedullin: a novel hypotensive peptide isolated from human pheochromocytoma. *Biochem Biophys Res Commun.* 1993;192:553–560.
30. Tokunaga N, Nagaya N, Shirai M, Tanaka E, Ishibashi-Ueda H, Harada-Shiba M, Kanda M, Ito T, Shimizu W, Tabata Y, Uematsu M, Nishigami K, Sano S, Kangawa K, Mori H. Adrenomedullin gene transfer induces therapeutic angiogenesis in a rabbit model of chronic hind limb ischemia: benefits of a novel nonviral vector, gelatin. *Circulation.* 2004;109:526–531.
31. Tsuruda T, Kato J, Kitamura K, Kawamoto M, Kuwasako K, Imamura T, Koiwaya Y, Tsuji T, Kangawa K, Eto T. An autocrine or a paracrine role of adrenomedullin in modulating cardiac fibroblast growth. *Cardiovasc Res.* 1999;43:958–967.
32. Nishikimi T, Yoshihara F, Horinaka S, Kobayashi N, Mori Y, Tadokoro K, Akimoto K, Minamino N, Kangawa K, Matsuoka H. Chronic administration of adrenomedullin attenuates transition from left ventricular hypertrophy to heart failure in rats. *Hypertension.* 2003;42:1034–1041.
33. Nakamura R, Kato J, Kitamura K, Onitsuka H, Imamura T, Cao Y, Marutsuka K, Asada Y, Kangawa K, Eto T. Adrenomedullin administration immediately after myocardial infarction ameliorates progression of heart failure in rats. *Circulation.* 2004;110:426–431.
34. Nagaya N, Satoh T, Nishikimi T, Uematsu M, Furuichi S, Sakamaki F, Oya H, Kyotani S, Nakanishi N, Goto Y, Masuda Y, Miyatake K, Kangawa K. Hemodynamic, renal, and hormonal effects of adrenomedullin infusion in patients with congestive heart failure. *Circulation.* 2000;101:498–503.
35. Fuller J, Mynett JR, Sugden PH. Stimulation of cardiac protein synthesis by insulin-like growth factors. *Biochem J.* 1992;282:85–90.
36. Florini JR, Ewton DZ, Coolican SA. Growth hormone and the insulin-like growth factor system in myogenesis. *Endocr Rev.* 1996;17:481–517.
37. Cittadini A, Stromer H, Katz SE, Clark R, Moses AC, Morgan JP, Douglas PS. Differential cardiac effects of growth hormone and insulin-like growth factor-1 in the rat: a combined in vivo and in vitro evaluation. *Circulation.* 1996;93:800–809.
38. Li Q, Li B, Wang X, Leri A, Jana KP, Liu Y, Kajstura J, Baserga R, Anversa P. Overexpression of insulin-like growth factor-1 in mice protects from myocyte death after infarction, attenuating ventricular dilation, wall stress, and cardiac hypertrophy. *J Clin Invest.* 1997;100:1991–1999.
39. von Lewinski D, Voss K, Hulsmann S, Kogler H, Pieske B. Insulin-like growth factor-1 exerts Ca^{2+}-dependent positive inotropic effects in failing human myocardium. *Circ Res.* 2003;92:169–176.
40. Thomas CV, Coker ML, Zellner JL, Handy JR, Crumbley AJ 3rd, Spinale FG. Increased matrix metalloproteinase activity and selective upregulation in LV myocardium from patients with end-stage dilated cardiomyopathy. *Circulation.* 1998;97:1708–1715.
41. Spinale FG, Coker ML, Krombach SR, Mukherjee R, Hallak H, Houck WV, Clair MJ, Kribbs SB, Johnson LL, Peterson JT, Zile MR. Matrix metalloproteinase inhibition during the development of congestive heart failure: effects on left ventricular dimensions and function. *Circ Res.* 1999;85:364–376.
42. Spinale FG, Coker ML, Heung LJ, Bond BR, Gunasinghe HR, Etoh T, Goldberg AT, Zellner JL, Crumbley AJ. A matrix metalloproteinase induction/activation system exists in the human left ventricular myocardium and is upregulated in heart failure. *Circulation.* 2000;102:1944–1949.
43. Kodama M, Matsumoto Y, Fujiwara M, Zhang SS, Hanawa H, Itoh E, Tsuda T, Izumi T, Shibata A. Characteristics of giant cells and factors related to the formation of giant cells in myocarditis. *Circ Res.* 1991;69:1042–1050.

CLINICAL PERSPECTIVE

Transplantation of stem or progenitor cells has the potential to improve and restore cardiac function. To date, experimenters investigating the possible therapeutic effects of stem cells in the heart have used models of infarction, and little information is available about the therapeutic potential of cell transplantation for heart failure due to dilated cardiomyopathy. In the present study, we demonstrated that transplantation of stem cells improved cardiac function in a model of myocarditis. We found evidence that stem cells may work to improve heart function by both myogenesis and angiogenesis while inhibiting myocardial fibrosis. Based on our data, part of the mechanism for this improvement may occur through the action of stem cells as a source of growth factors and cytokines in the heart. This study supports the overall notion that mesenchymal stem cells transplanted into the failing heart have potential as a new therapeutic strategy for the treatment of dilated cardiomyopathy.

Tomohiro Makino[1]
Masaru Matsumoto[1]
Yuji Suzuki[1]
Yasuo Kitajima[1]
Katsuhiko Yamamoto[1]
Masashi Kuramoto[1]
Yoshiharu Minamitake[1]
Kenji Kangawa[2]
Masayuki Yabuta[1]
[1] *Institute for Medicinal Research and Development, Daiichi Suntory Pharma Co., Ltd. Chiyoda, Ohra, Gunma 370-0503, Japan*

[2] *Department of Biochemistry, National Cardiovascular Center Institute, Suita, Osaka, 565-8565, Japan*

Semisynthesis of Human Ghrelin: Condensation of a Boc-Protected Recombinant Peptide with a Synthetic *O*-Acylated Fragment

Received 12 May 2005; revised 4 July 2005; accepted 11 July 2005
Published online 27 July 2005 in Wiley InterScience (www.interscience.wiley.com). DOI 10.1002/bip.20342

Abstract: *The creation of peptide using a combination of recombinant expression and chemical synthesis can be a powerful tool for the production of a wide variety of polypeptides modified by phosphorylation, glycosylation, etc. We have developed a new method for the preparation of a recombinant peptide with a free* N^{α}*-amino group and protected* N^{ε}*-amino groups, and have used this method in the semisynthesis of human ghrelin. Ghrelin, a natural ligand for growth hormone secretagogue receptor, is a 28-residue peptide with an essential* n*-octanoyl modification on Ser3. A 7-residue N-terminal fragment of ghrelin containing the octanoyl modification was prepared by Fmoc chemistry. In the preparation of it, all reactions were performed on the 2-chlorotrityl resin. Additionally, TBDMS and tBu turned out to be the most effective protection groups for the Ser3 and the Ser2, Ser6, respectively. For preparation of a 21-residue C-terminal fragment, we established a two-step protease processing method for the partially protected segment. A recombinant precursor peptide was Boc protected and subsequently cleaved using two distinct proteases, OmpT and Kex2. The peptides were then coupled to each other and, after deprotection, resulted in fully active human ghrelin.* © 2005 Wiley Periodicals, Inc. Biopolymers 79: 238–247, 2005

This article was originally published online as an accepted preprint. The "Published Online" date corresponds to the preprint version. You can request a copy of the preprint by emailing the Biopolymers editorial office at biopolymers@wiley.com

Keywords: *ghrelin; semisynthesis; two-step protease processing; OmpT and Kex2; 2-chlorotrityl resin*

Correspondence to: T. Makino; e-mail: tomohiro_makino@asabio.co.jp

Biopolymers, Vol. 79, 238–247 (2005)

INTRODUCTION

Technological advancements have spurred the pharmaceutical development of many physiological peptides and proteins such as insulin, growth hormone, and calcitonin.[1–3] Both chemical synthesis and recombinant expression are used for their large-scale manufacture.[4,5] However, establishing methods for the mass production of modified peptides or proteins remains challenging. Although chemical synthesis methods can surely be utilized, they have the disadvantage of limits on peptide size and the difficulty of maintaining cost performance and a constant supply.

Genetic recombination is a useful method suitable for mass production, but prokaryotes such as *Escherichia coli* cannot produce modified peptides. Even when using eukaryotes such as yeast or mammalian cell lines, it is still difficult to control the modification of specific amino acids and to apply the method for mass production. Therefore, by combining chemical synthesis and genetic recombination, a semisynthesis method can be achieved that utilizes the advantages of both.

Ghrelin is novel gastrointestinal hormone that stimulates growth hormone (GH) release, guts motilities and food intake, and is responsible for positive energy balance.[6–8] It is an acylpeptide consisting of 28 amino acids with Ser3 esterified with octanoic acid (Figure 1). This modification is essential for its biological activity.[6] Although many acylated proteins have been reported,[9–11] ghrelin is the first acylated peptide known to have hormonal activities in mammals.

In the case of ghrelin, chemical synthesis can readily produce this peptide,[12,13] but it has been deemed economically inefficient. Because of its posttranslational modification, it cannot be synthesized by prokaryotic cells. In addition, it would still be difficult to use eukaryotes because ghrelins also become esterified with butanoic acid (C4), decanoic acid (C10), or their unsaturated fatty acids.[14] By using this newly developed semisynthetic method, we have established an efficient method of production for ghrelin.

MATERIALS AND METHODS

Synthesis of the ([N^{α}-t-butyloxycarbonyl (Boc), Ser t-butyl (tBu))^{2,6}]hGhrelin(1-7)) N-terminal Fragment

A prolyl-2-chlorotrityl resin (46.52 g, 20.0 mmoL, Novabiochem®) was placed into a glass vessel reactor. The construction of Boc-Gly-Ser(*t*Bu)-Ser(*t*-butyl dimethylsilyl (TBDMS))-Phe-Leu-Ser(*t*Bu)-Pro-2-chlorotrityl resin was accomplished by repeated introductions of fluorenylmethoxycarbonyl (Fmoc)-amino acids with 2-(1*H*-benzotriazole-1-yl)-1,1,3,3,-

FIGURE 1 Structure of human ghrelin.

tetramethyluronium hexafluorophosphate (HBTU) and 1-hydroxybenzotriazole and removal of the Fmoc with 20% piperidine/*N*-methyl-2-pyrrolidone (NMP). The protected peptide resin was treated with 0.1 *M* tetrabutylammonium fluoride (TBAF)/ *N,N*-dimethylformamide (DMF) (400 mL) at room temperature for 30 min, filtered, and washed successively with DMF and NMP. The resulting de-TBDMS peptide resin was reacted with octanoic acid (11.56 g) in NMP (163 mL) and 1-ethyl-3-(3-dimethylaminopropyl)carbodiimide (EDC)·HCl (16.90 g) was added in the presence of 7.33 g of 4-dimethylaminopyridine (DMAP). After stirring for 18 h, the resin was filtered and washed with NMP. 300 mL of 0.1% trifluoracetic acid (TFA), 20% trifluoroethanol/ dichloromethane then was added and stirred for 30 min at room temperature to cleave the peptide from the resin. After filtration and concentration, 200 mL of H_2O was added to precipitate, the peptides were washed with H_2O and hexane and were filtered again and dried under reduced pressure to obtain 18.74 g (yield, 91%) of the N-terminal fragment ([N^{α}-Boc, Ser (*t*Bu)^{2,6}]hGhrelin(1-7)).

Expression of the hGhrelin(8-28) Derivative

A cDNA encoding amino acids of human ghrelin(8-28)[6] was produced using an annealing method with a synthetic DNA oligonucleotide (Sigma Aldrich Japan, Tokyo, Japan). The p117s8-28ok plasmid is a pBR322-based vector that expresses amino acids of the ghrelin(8-28) as a fusion protein under the control of the *E. coli lac* promoter. The fusion protein consists of three parts: the N-terminal 117 amino acids of *E. coli* β-galactosidase,[15] linker amino acids designed for protease digestions, and amino acids of the ghrelin(8-28). A schematic of the structure of p117s8-28ok and nomenclature of the ghrelin(8-28) fusion proteins used in this study are shown in Figure 3. The expression plasmids were transformed into *E. coli* strain W3110.

Preparation of the ([Lys(Boc)^{16,19,20,24}] hGhrelin(8-28)) C-terminal Fragment

Fusion proteins were expressed in *E. coli* W3110 as inclusion bodies. After cultivation in a 20-L fermenter at 37°C for 30 h, the cells were lysed by two passes through a high-pressure homogenizer. The cell debris and inclusion bodies were pelleted by centrifugation (6,500*g*, 30 min) and resuspended in 820 mL of deionized water. The inclusion body suspension (820 mL) was subjected to the OmpT protease[16] in 9 L of 4 *M* urea, 20 mM Tris–HCl (pH 7.4), and 50 mM NaCl at 32°C. Afterward, the residue was removed by centrifugation (9,000*g*, 30 min) and the supernatant was purified by cation exchange chromatography. The hGhrelin(8-28) precursor (12.8 g) was eluted in 1.25 L of 1.5 *M* urea, 0.5 *M* NaCl, and

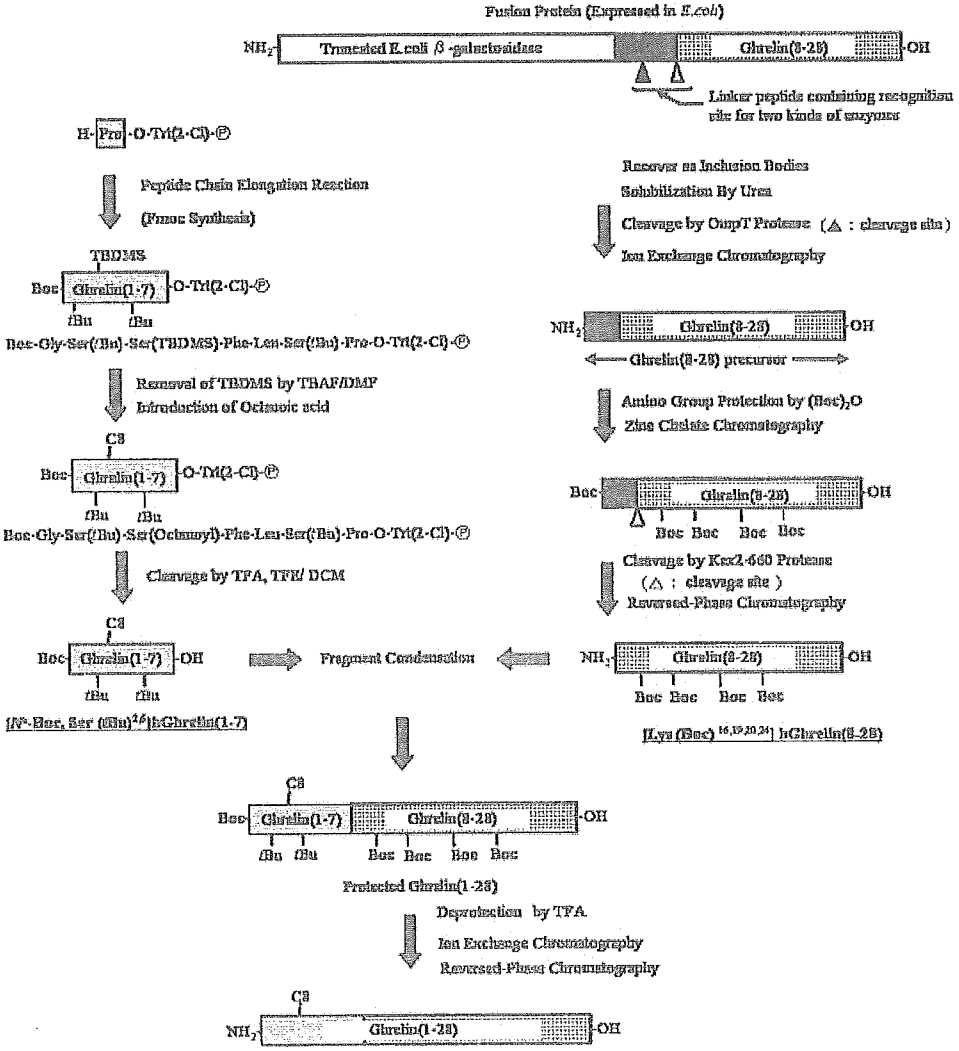

FIGURE 2 Scheme of semisynthesis of human ghrelin.

50 mM $NaHCO_3$ (pH 11). Purified hGhrelin(8-28) precursor was Boc-protected in 3.57 L of 30% acetonitrile (MeCN) and 20 mM $(Boc)_2O$ (pH 10) for 2 h at room temperature. The [N^{α}-Boc, Lys(Boc)^{16,19,20,24}]hGhrelin(8-28) precursor was purified by Zn^{2+} chelate chromatography and eluted by 3.36 L of 0.1 *M* imidazole, and 20 mM Tris–HCl (pH 6.4). Next, the purified precursor was digested with the second protease, Kex2-660 (52,900 unit/mL), a soluble form of Kex2.[17] The reaction was carried out in 3.57 L of 5 mM $CaCl_2$ (pH 8.3) at 37°C. After the reaction, [Lys(Boc)^{16,19,20,24}]hGhrelin(8-28) was purified by reversed-phase chromatography. The peptide was eluted by a linear gradient from solvent A (10% MeCN, 0.1% TFA) to solvent B (50% MeCN, 0.1% TFA). The eluent (5.95 g, 730 mL) was lyophilized for storage.

Condensation and Deprotection

[N^{α}-Boc, Ser(*t*Bu)^{2,6}]hGhrelin(1-7) and [Lys(Boc)^{16,19,20,24}]h Ghrelin(8-28) were subjected to a condensation reaction. [N^{α}-Boc, Ser(*t*Bu)^{2,6}]hGhrelin(1-7) (1.67 g, 1.6 mmol), HBTU (0.62 g, 1.6 mmol), and diisopropylethylamine (0.3 mL, 1.6 mmol) were dissolved in 8.3 mL of DMF and the solution was stirred for 30 min. [Lys(Boc)^{16,19,20,24}]hGhrelin(8-28) (5.53 g, 1.4 mmol) was dissolved in 27.7 mL of DMF, and the activated N-terminal fragment solution was added by drops while stirring at room temperature. After 90 min, the reaction solvent was evaporated under reduced pressure. TFA (52.8 mL) was added to the resulting residue, and the mixture was slowly stirred at room temperature for 3 h. The TFA was evaporated under reduced pressure, and 150 mL of isopropylether was added to the residue to obtain precipitates, which were washed and dried to obtain 6.26 g of white, powdery crude peptide.

Purification of Human Ghrelin

After synthesis, crude human ghrelin (3.32 g) was dissolved in 500 mL of 5% acetic acid, followed by ion exchange chromatography. Human ghrelin was eluted by 250 mL of 0.5 *M* NaCl and 50 mM AcONa (pH 5). The eluent (3.29 g) was

Table I Optimization of TBDMS Group Removal

	TBAF (*M*)	Reaction Time (h)	Yield[a] (%)	Purity of Desired Product[b] (%)	Ratio[b] Octanoy : Desoctanoyl
I	0.01	0.25	89	94	98.3 : 1.7
II	0.01	3	100	97	100 : ND[c]
III	0.1	0.25	94	97	100 : ND
IV	0.1	0.5	100	96	100 : ND
V	0.1	1	98	96	100 : ND
VI	0.1	3	100	96	100 : ND

[a] Calculated based on a substitution rate of a prolyl-2-chlorotrityl resin.
[b] Purity and rate determined by analytical HPLC.
[c] ND, not detected.

then further purified by reversed-phase chromatography. The purified peptide was eluted by linear gradient from solvent A (50 mM acetic acid (AcOH) to solvent B (60% MeCN and 50 mM AcOH). Final yield of purified ghrelin was 2.60 g.

Detection of Ghrelin Activity by Calcium Mobilization Assay

The assay was performed according to the method described by Hosoda et al.[14] with minor modifications. CHO cells were used to express the GHS-Receptor. Inner calcium concentration ($[Ca^{2+}]$) changes were measured with a fluorometric imaging plate reader (FLEXstation; Molecular Devices Inc., Sunnyvale, CA, USA). Maximum changes in fluorescence, compared to baseline measurements, were used to determine the level of agonist response. Synthetic human ghrelin was purchased from Peptide Institute Inc. (Osaka, Japan).

Preparative Columns Used

Ion exchange chromatography resin (SP Sepharose Big Beads), chelate chromatrography resin (Chelating Sepharose Fast Flow), and reversed-phase chromatography resin (Source 30RPC) were all purchased from Amersham Biosciences, Inc. (Piscataway, NJ, USA).

Analytical HPLC

A Shimadzu LC-10A System was used. Columns were YMC-Pack PROTEIN-RP, YMC-Pack ODS AP-302, and YMC-Pack PROTEIN-C8 (all 4.6 mmϕ × 150 mm; manufactured by YMC Co., Ltd., Kyoto, Japan). Eluent condition: In 0.1% TFA, the MeCN concentration was linearly changed to a maximum of 100%. Flow rate: 1 mL/min. Detection: UV (210 or 214 nm).

Preparative Chromatography System

An AKTA explorer 10S chromatography system and an AKTA PILOT chromatography system (Amersham Biosciences, Inc.) were used.

Mass Spectrometry

A Finnigan MAT Corporation TSQ7000 instrument was used. Ion source: ESI; detection ion mode: positive; spray voltage: 4.5 kV; capillary temperature: 250°C; mobile phase: 0.2% AcOH–methanol (1:1) solution; flow rate: 0.2 mL/min; scan range: *m/z* from 300 to 1,500.

Table II Optimization of Reaction Conditions for Octanoylating Serine3[a]

	Octanoic Acid (equivalent)	EDC (equivalent)	DMAP (equivalent)	Reaction Time (h)	Yield[b] (%)	Purity of Desired Product[c] (%)	Ratio[c] Octanoyl : Desoctanoyl
VII	4	4.4	0.1	24	83	94	97.2 : 2.8
VIII	2	2.2	1	24	93	96	99.5 : 0.5
IX	4	4.4	1	1	85	78	80.5 : 19.5
X	4	4.4	1	4	98	97	99.7 : 0.3
XI	4	4.4	1	8	98	96	100 : ND[d]
XII	4	4.4	1	16	97	98	100 : ND

[a] All samples were treated with 0.1 *M* TBAF for 1 h, to remove a TBDMS group.
[b] Calculated based on a substitution rate of a prolyl-2-chlorotrityl resin.
[c] Purity of desired product and rate of production were calculated using analytical HPLC.
[d] ND, Not detected.

Table III Amino Acid Composition and Mass Spectrometry of [N^{α}-Boc, Ser(tBu)^{2,6}] hGhrelin(1-7) and [Lys(Boc)^{16,19,20,24}]hGhrelin(8-28)

	[N^{α}-Boc, Ser(tBu)^{2,6}]h Ghrelin(1-7)	[Lys(Boc)^{16,19,20,24}]h Ghrelin(8-28)
ESI-MS	1032.6 (theoretical value 1032.3)	2969 (theoretical value 2969.4)
Amino Acid Composition Ratio	Gly; 1.01 (1), Leu; 1(1), Phe; 0.99 (1), Pro; 1.00 (1), Ser, 2.70 (3)[a]	Ala; 1.01 (1), Arg; 2.84 (3), Glx; 5.75 (6), His; 0.92 (1), Leu; 1 (1), Lys; 3.92 (4), Pro; 2.92 (3), Ser; 0.90 (1), Val; 0.94 (1)

[a] Values in parentheses are theoretical.

Amino Acid Sequence Analysis

An Applied Biosystems 477A sequencer (Perkin–Elmer, Yokohama, Japan) was used.

Amino Acid Ccomposition Analysis

An L-8500 amino acid analyzer (Hitachi, Ltd., Tokyo, Japan) was used. The sample was hydrolyzed with 6 *M* HCl containing 0.1% phenol at 110°C for 24 h in a sealed tube.

RESULTS

Complete Scheme of the Semisynthesis of Ghrelin

The strategy of producing semisynthetic ghrelin is described in Figure 2. The N-terminal fragment containing C8 modification was chemically synthesized. Starting with a prolyl-2-chlorotrityl resin, the peptide

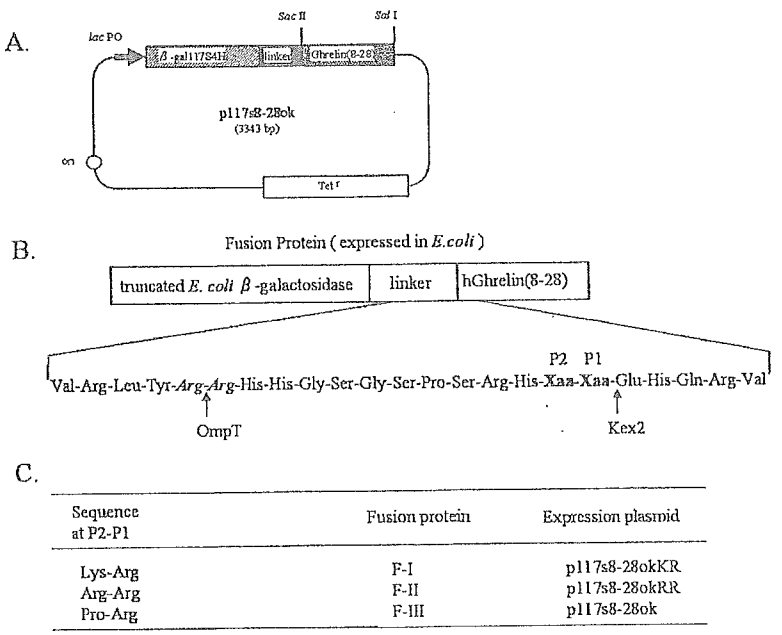

C.

Sequence at P2-P1	Fusion protein	Expression plasmid
Lys-Arg	F-I	p117s8-28okKR
Arg-Arg	F-II	p117s8-28okRR
Pro-Arg	F-III	p117s8-28ok

FIGURE 3 (A) Construction of a human ghrelin(8-28) fusion protein expression plasmid (p117s8-28ok). *lac*PO, lac promoter; Tet^{r}, tetracycline resistant gene; ori, replication start point; Ghrelin(8-28), synthetic DNA oligo encoding human ghrelin(8-28); β-gal117S4H, DNA sequence of *E. coli* β-galactosidase derivative. (B) Schematic representation of human ghrelin(8-28) fusion protein with the amino acid sequences of the cleavage sites. The arrow indicates the cleavage site of OmpT and Kex2-660. The substrate residues of Kex2 are denoted as P1, P2, starting from the N-terminal side of the cleavage sites. Xaa-Xaa at P2, P1 represents an amino acid sequence. The first-round peptidase, OmpT, recognizes italic Arg-Arg and cuts at the center of them. The second-round peptidase, Kex2, recognizes the bold Xaa-Xaa and cuts the C-terminal of it. (C) Nomenclature of the fusion proteins and plasmids. Several expression plasmids were constructed that encode each fusion protein in which the P2-P1 site was changed.

backbone was synthesized by Fmoc chemistry, giving Boc-Gly-Ser(*t*Bu)-Ser(TBDMS)-Phe-Leu-Ser(*t*Bu)-Pro-2-chlorotrityl-resin. After treatment of the peptide–resin with TBAF, and followed by acylation, the N-terminal fragment was obtained after cleavage from the resin. For synthesis of the C-terminal fragment (21 a.a.), starting with the recombinantly produced precursor, the combination of two distinct proteases (OmpT and Kex2) and Boc protection of amino groups enabled efficient preparation of a fragment that was suitable for coupling with the N-terminal fragment. After the two segments underwent condensation, deprotection, and purification, highly purified human ghrelin was produced.

Synthesis of [N^{α}-Boc, Ser(tBu)^{2,6}] hGhrelin(1-7)

To avoid possible racemization upon coupling with the C-terminal portion of ghrelin, the Pro7 was selected as a coupling site. Several synthetic approaches were tried, and a variety of protecting groups were tested for the Ser side chains. The best result was obtained via protection with TBDMS at the Ser3 and with *t*Bu at the Ser2 and Ser6. Treatment of the peptide–resin with TBAF was followed by acylation, after which the peptide–resin was treated with diluted TFA to give the desired fragment. Over the course of many synthetic trials, the conditions for removal of the TBDMS group and for acylation were optimized (Tables I and II). As a result, it was clear that the removal reaction of the TBDMS group is best when performed for 30 min to 1 h using a 0.1 *M* TBAF solution and that the octanoylation reaction should be performed for 8 to 16 h using 4 equivalents of octanoic acid, 4.4 equivalents of EDC, and 1 equivalent of DMAP.

The purity of this product was analyzed by HPLC (see Figure 7(1)A) and found to be 90%. This product was shown to possess the same amino acid composition and molecular mass as the theoretical value (Table III).

Preparation of [Lys(Boc)^{16,19,20,24}]hGhrelin(8-28)

To perform the most efficient condensation and to suppress side reactions, we needed to prepare a partially protected peptide whose N-terminal α-amino group was free while all other side chain amino groups were blocked. We employed two proteases, OmpT and Kex2, to process the target peptide from fusion protein. The fusion protein consists of truncated *E. coli* β-galactosidase followed by the target peptide with a linker designed to allow cleavage with these two proteases. The schematic representation of this protein is shown in Figure 3.

Previous studies have reported that cleavage efficiency of Kex2 largely depends on the substrate sequence, especially of the P1, P2 sites (Figure 3).[18,19] Therefore, we first used PCR to construct several expression vectors of the fusion protein, using the p117s8-28ok plasmid as a template (Figure 3). We found that the most efficient reaction occurred with fusion protein "F-II," whose P2-P1 site is Arg-Arg (Table IV). The "F-II" protein, encoded by the p117s8-28okRR plasmid, was chosen and used for the following experiments.

The F-II fusion protein was successfully expressed as an inclusion body in *E. coli*. The fusion proteins were subjected to treatment with OmpT protease under denaturing conditions. As the *E. coli* W3110 strain encodes this protease, it cleaves the fusion protein on solubilization by urea,[20] resulting in the generation of the C-terminal portion of ghrelin with a linker peptide at its N-terminus (Figure 4). The cleavage efficiency was around 90%. After purification by cation exchange chromatography, the α-amino group at the N-terminal and the side chain Lys residues were protected by Boc groups (Figure 5). As the peptide increased the hydrophobicity during the reaction, extension of the retention time was observed (Figure 5).

This reaction's efficiency was about 95%. After purification by Zn^{2+} chelate chromatography, the peptide was subjected to digestion with the Kex2 protease (Figure 6), releasing [Lys(Boc)^{16,19,20,24}]hGhrelin (8-28) with a free N^{α}-amino group. The cleavage efficiency was nearly 90%. Though we optimized the linker sequence suitable for Kex2 protease, we observed extra cleavage in this reaction (Figure 6,

Table IV Cleavage Efficiency of Kex2 Protease to Various Fusion Proteins

Fusion Protein	Kex2 Units Necessary To Cleave each Fusion Protein (1 mg/mL)
F-I[a]	Not cleaved[b]
F-II[a]	1.0×10^4 unit/mL[c]
F-III[a]	1.2×10^5 unit/mL[c]

[a] Construction of each fusion protein shown in Figure 3. Plasmids were constructed by PCR using p117 8-28oPR as a template.

[b] Cleavage did not occur due to masking of the positive charge of Lys by Boc.

[c] One unit was defined as an amount of the enzyme that releases 1 pmol AMC (7-amino-4-methylcoumarin) per minute from Boc-Leu-Arg-Arg-MCA (4-methylcoumaryl-7-amide). Details are described by Mizuno *et al.*[17]